

# SegEarth-R2: Towards Comprehensive Language-guided Segmentation for Remote Sensing Images

Zepeng Xin<sup>1\*</sup>, Kaiyu Li<sup>1\*</sup>, Luodi Chen<sup>1</sup>, Wanchen Li<sup>1</sup>, Yuchen Xiao<sup>1</sup>, Hui Qiao<sup>2</sup>,  
Weizhan Zhang<sup>1</sup>, Deyu Meng<sup>1</sup>, Xiangyong Cao<sup>1†</sup>

<sup>1</sup>Xi'an Jiaotong University <sup>2</sup> China Telecom Shaanxi Branch

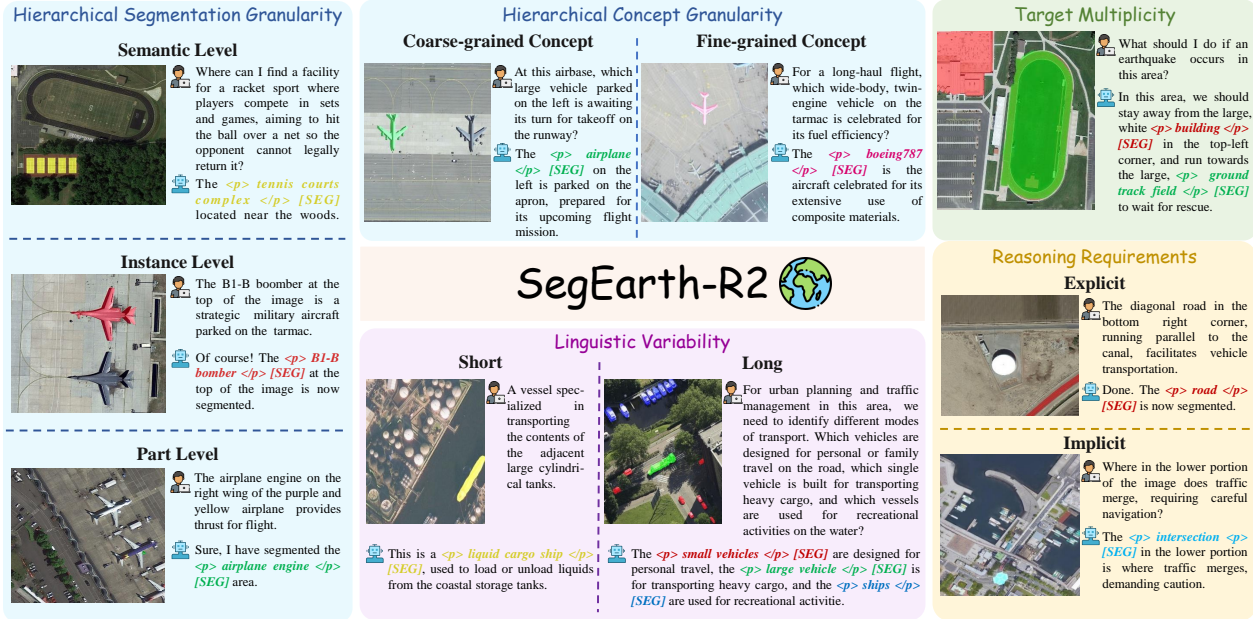


Figure 1. SegEarth-R2 can handle various language-guided segmentation in remote sensing across four key dimensions: (1) **Hierarchical Granularity**; (2) **Target Multiplicity**; (3) **Reasoning Requirements**; and (4) **Linguistic Variability**.

## Abstract

Effectively grounding complex language to pixels in remote sensing (RS) images is a critical challenge for applications like disaster response and environmental monitoring. Current models can parse simple, single-target commands but fail when presented with complex geospatial scenarios, e.g., segmenting objects at various granularities, executing multi-target instructions, and interpreting implicit user intent. To drive progress against these failures, we present LaSeRS, the first large-scale dataset built for comprehensive training and evaluation across four critical dimensions of language-guided segmentation: hierarchical granularity, target multiplicity, reasoning requirements, and linguistic variability. By capturing these dimensions, LaSeRS moves beyond simple commands, providing

a benchmark for complex geospatial reasoning. This addresses a critical gap: existing datasets oversimplify, leading to sensitivity-prone real-world models. We also propose SegEarth-R2, an MLLM architecture designed for comprehensive language-guided segmentation in RS, which directly confronts these challenges. The model's effectiveness stems from two key improvements: (1) a spatial attention supervision mechanism specifically handles the localization of small objects and their components, and (2) a flexible and efficient segmentation query mechanism that handles both single-target and multi-target scenarios. Experimental results demonstrate that our SegEarth-R2 achieves outstanding performance on LaSeRS and other benchmarks, establishing a powerful baseline for the next generation of geospatial segmentation. All data and code will be released at <https://github.com/earth-insights/SegEarth-R2>.

\*Equal contribution

†Corresponding author (caoxiangyong@mail.xjtu.edu.cn)

## 1. Introduction

Imagine you are walking in a park when the ground begins to shake violently—an earthquake. Immediately, instinct kicks in and your mind swiftly translates the abstract goal of “finding a safe refuge” into a complex, spatially-aware plan (e.g., the target multiplicity case depicted in Figure 1): simultaneously identifying the nearby, open **ground track field** (the safe destination) while also urgently moving away from the surrounding **tall, swaying buildings** (the hazards). This remarkable human ability to ground a high-level, compound instruction into a precise, multi-target, pixel-level action is vital for survival. Yet, it is precisely this ability that even advanced AI systems for Earth observation struggle to replicate. While these systems excel at executing literal commands [9, 23, 25, 27, 28, 36, 41, 50, 72, 79], they fall short when interpreting abstract natural language that requires understanding spatial relationships between multiple targets, especially in the context of precise language-guided segmentation in complex, real-world remote sensing (RS) environments.

This inability to interpret complex instructions directly hinders the deployment of advanced geoinformation systems. Indeed, language-guided segmentation holds immense promise across diverse and complex real-world RS applications, including environmental dynamics, urban planning, and, critically, disaster management [1, 3, 7, 26, 39, 45, 49, 58]. However, its development has been significantly inhibited by the lack of comprehensive training and evaluation resources. Specifically, existing datasets do not adequately capture the full range of required complexity, such as segmenting objects across hierarchical granularity and handling complex target multiplicity instructions.

To address these critical gaps, we introduce LaSeRS, a large-scale dataset of over 40k high-quality masks and 30k QA pairs, generated via a scalable semi-automated annotation pipeline. As illustrated in Figure 1, LaSeRS is constructed to serve as a comprehensive training and evaluation resource across the four dimensions of RS language-guided segmentation. Unlike prior works limited to single-target and explicit queries, LaSeRS systematically incorporates: **Hierarchical Granularity**, requiring both conceptual (coarse- to fine-grained) and segmentation (semantic to part-level) precision; **Target Multiplicity**, where a single instruction demands grounding of multiple objects; **Reasoning Requirements**, both explicit descriptions and challenging implicit instructions; and **Linguistic Variability**, spanning concise short queries and highly detailed long descriptions. Further, LaSeRS significantly pushes scale, offering more than 5 $\times$  the category coverage of existing RS datasets [9, 28, 29, 36, 79], thereby significantly expanding the boundary of language-guided segmentation in RS.

The LaSeRS dataset poses some critical challenges to existing models [19, 28, 50, 62], motivating the introduction

of our SegEarth-R2 model. We built our model to overcome two primary failures. First, existing methods struggle with fine-grained segmentation of small and part-level object in LaSeRS. SegEarth-R2 confronts this with a spatial attention supervision mechanism, enforcing an internal focus on precise details. Second, grounding multiple targets from a single instruction is inefficient or unsupported by previous query designs [28]. SegEarth-R2 address this with a flexible segmentation query mechanism capable of dynamically handling both single and multi-target requests.

In summary, our contributions are as follows:

- We introduce LaSeRS, the first benchmark for training and evaluation comprehensive language-guided segmentation in RS across four critical dimensions spanning hierarchical granularity, target multiplicity, reasoning requirements, and linguistic variability.
- We propose SegEarth-R2, a effective MLLM architecture for comprehensive language-guided segmentation in RS. It incorporates a spatial attention supervision for precise fine-grained localization and a flexible query mechanism for handling multi-target instructions.
- SegEarth-R2 sets a new state-of-the-art on LaSeRS and other public benchmarks. With only 3B parameters, it demonstrates superior performance against larger models, establishing a powerful yet highly efficient baseline for the comprehensive language-guided segmentation.

## 2. Related works

**Multimodal Large Language Models (MLLMs).** MLLMs build upon Large Language Models (LLMs) to acquire vision capabilities. In the general domain, pioneers like LLaVA [24, 32, 33] and InstructBLIP [6] aligned visual features with language representations using a vision-language connector, enhanced by instruction tuning. While these initial models focused on image-level understanding, subsequent works like GPT4RoI [75] and RegionGPT [10] advanced this by introducing regional understanding. This evolution is mirrored in the RS domain, where MLLMs have evolved from foundational conversational agents like RSGPT [14]. Subsequent RS-specific models have integrated more complex functionalities. For instance, GeoChat [18] supports region-specific inputs and visual grounding through oriented bounding box coordinates in its responses. Others extend capabilities to RS-video captioning, such as SkyEyeGPT [73], or integrate multi-sensor tasks, as exemplified by EarthGPT [76] and EarthDial [52]. However, despite these advances in interpretation [2, 15, 30, 42] and relation reasoning [43, 55, 73], a fundamental limitation persists: these models lack crucial pixel-level understanding and segmentation capabilities.

**Language-guided Segmentation.** Language-guided segmentation refers to locating target regions at the pixel level from natural language, including referring segmen-

Table 1. Comparison between LaSeRS and other related datasets. TI: Textual Instruction, TA: Textual Answer, BBox: Bounding Box, Seg: Segmentation Mask. LaSeRS outperforms other datasets with the largest number of classes and unique support for **Hierarchical Granularity**, **Target Multiplicity**, **Reasoning Requirements**, and **Linguistic Variability**.

| Dataset          | Masks  | Class Num | Annotation Type   | Hierarchical Segmentation | Granularity Concept | Target Multiplicity Single | Multiple | Reasoning Requirements Explicit | Implicit | Linguistic Variability Long | Short |
|------------------|--------|-----------|-------------------|---------------------------|---------------------|----------------------------|----------|---------------------------------|----------|-----------------------------|-------|
| EarthVQA [57]    | 6,000  | 14        | TI, TA            | ✗                         | ✗                   | ✓                          | ✓        | ✓                               | ✓        | ✗                           | ✓     |
| RegSegRS [72]    | 4,420  | 14        | TI, Seg           | ✗                         | ✗                   | ✓                          | ✗        | ✓                               | ✗        | ✗                           | ✓     |
| RRSIS-D [36]     | 17,420 | 20        | TI, Seg, BBox     | ✗                         | ✗                   | ✓                          | ✗        | ✓                               | ✗        | ✗                           | ✓     |
| RISBench [9]     | 52,472 | 26        | TI, Seg, BBox     | ✗                         | ✗                   | ✓                          | ✗        | ✓                               | ✗        | ✗                           | ✓     |
| EarthReason [28] | 5,434  | 28        | TI, TA, Seg       | ✗                         | ✗                   | ✓                          | ✗        | ✗                               | ✓        | ✓                           | ✗     |
| LaSeRS           | 40,396 | 122       | TI, TA, Seg, BBox | ✓                         | ✓                   | ✓                          | ✓        | ✓                               | ✓        | ✓                           | ✓     |

tation [8, 12, 34, 59, 65, 67, 81] and reasoning segmentation [16, 19, 48, 81]. In RS, RefSegRS [72] introduced the first referring segmentation dataset, while RRSIS-D [36] and some subsequent works [9, 41, 41, 68, 79, 79] expanded dataset scale and enriched prompts, though still limited to explicit category queries. EarthReason [28] further introduced geospatial pixel reasoning with the first reasoning segmentation dataset for Earth observation. Yet, while a valuable step, it primarily focuses on implicit reasoning for single targets, leaving the complex challenges of multi-granularity (e.g., part-level and fine-grained concept) and multi-target grounding unaddressed. To bridge this gap, LaSeRS offers a more comprehensive benchmark that systematically incorporates all of these critical dimensions.

**MLLMs for language-guided segmentation.** Recent work has explored leveraging the reasoning capabilities of MLLMs for complex language-guided segmentation. In the general domain, a dominant approach employs MLLMs as a reasoning engine to provide prompt embeddings (e.g., [SEG] tokens) for SAM [17, 47], thereby integrating reasoning into mask generation [11, 16, 19, 60, 64, 66, 71]. Other methods follow pipelines inspired by Mask2Former [4] (“propose-then-select”) [56, 61, 62, 65, 77] or treat segmentation as text generation [20, 21]. However, these general-purpose methods often underperform on RS datasets, which are characterized by the prevalence of small objects and significant scale variations. This has spurred the development of specialized MLLMs for the RS field [37, 40, 41, 51, 69, 79], with methods like GeoPixel [50] adapting grounded conversation, SegEarth-R1 [28] and LISAt [44] handling implicit queries, Geo-R1 [78] and RemoteReasoner [70] exploring reinforcement learning. Despite these advances in RS-specific models, they still lack the ability to handle language-guided segmentation in complex scenarios, such as multi-target settings or multi-granularity (e.g., part-level).

### 3. LaSeRS Dataset

#### 3.1. Data Generation and Filtering

We develop a four-stage semi-automatic data generation pipeline to generate question-answer-mask triples, as shown

in Figure 2. More details about the dataset construction can be found in the Suppl. 7.

**Stage 1: Masks Generation.** Our mask annotations are sourced from two complementary workflows. First, we incorporate masks from the existing SAMRS [54] dataset. However, these annotations exhibit varying quality and are limited to  $\sim 60$  categories. Second, to expand coverage and introduce part-level details, we use SAM [17] to generate masks for the entire image using a grid of point prompts. Then, for common RS object categories like airplanes and ships, we cropped the object region and apply a denser grid of prompts within that region to produce more refined, part-level masks. This stage generates a large volume of coarse masks that require subsequent filtering.

**Stage 2: Masks Filtering.** To ensure annotation quality, we apply distinct filtering methods based on the mask source. For masks originating from SAMRS, we discard samples where the number of connected components in a mask does not match the number of provided bounding box annotations. Given that objects in remote sensing images often exhibit clear geometric properties (e.g., the pronounced symmetry of airplanes and the rotational invariance typical of intersections), we then conduct geometric feature matching to filter out candidates that deviate significantly from a curated set of ideal, category-specific reference shapes (details in the Suppl. 7.3). In contrast, all masks generated by the second workflow are manually reviewed. Annotators assess each mask based on two criteria: semantic coherence, to ensure it represents a meaningful object, and high boundary quality, to ensure mask precision. This stage yields approximately 50K high-quality, semantically meaningful masks at varying segmentation granularities, from semantic- and instance-level to part-level.

**Stage 3: QAs Generation.** We used Gemini-2.5-pro [5] to create question-answer pairs, with the process differing based on the mask source. For masks with pre-existing category annotations from SAMRS, we leverage this information to guide the generation of diverse textual annotations. Conversely, for unlabeled masks from our second workflow, we first employ a prompting strategy to assign a category to each mask. This assigned category subsequently guides the generation of varied textual annotations. In both cases, we

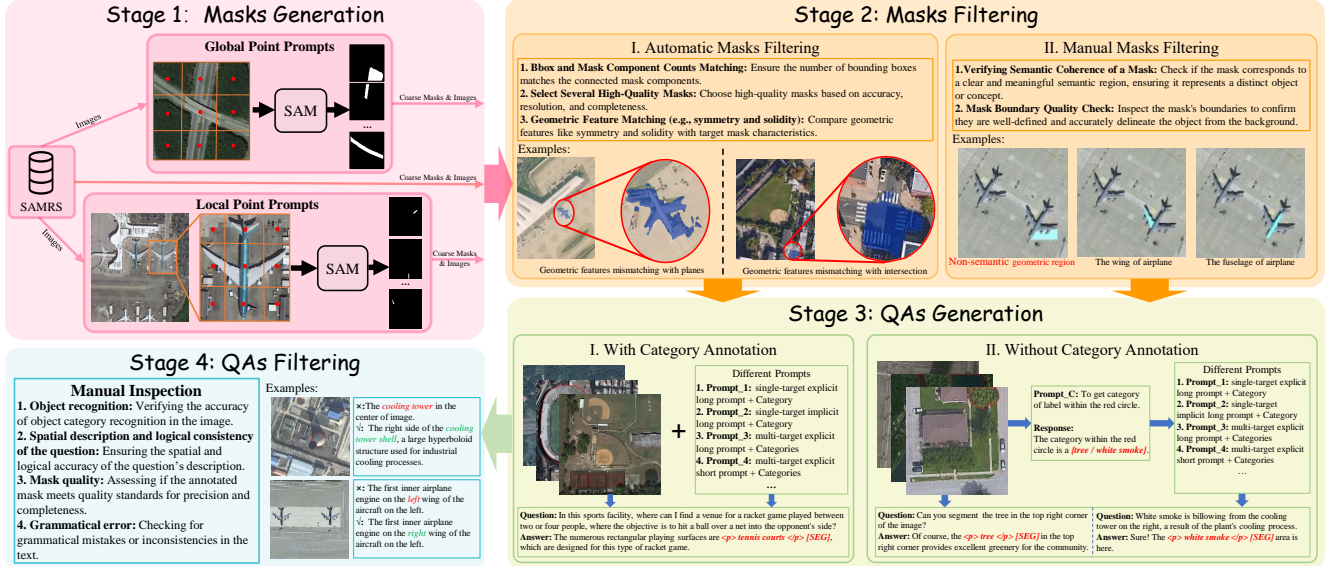


Figure 2. Overview of the construction of LaSeRS. Our scalable, semi-automatic annotation pipeline comprises four stages: two dedicated to data generation and two dedicated to filtering. Data quality is rigorously ensured through both automatic and manual verification.

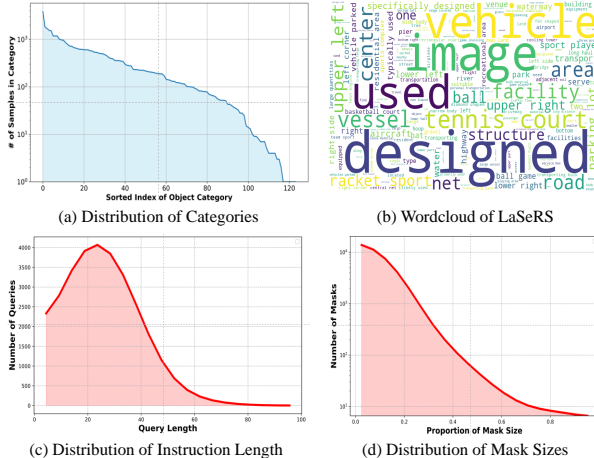


Figure 3. Data Statistics of LaSeRS.

utilize multiple prompt templates to create question-answer pairs of varying styles, including explicit vs. implicit and detailed vs. concise. This stage ultimately yields approximately 40K question-answer pairs. However, due to potential hallucinations from the Gemini-2.5-pro, these pairs require further filtering.

**Stage 4: QAs Filtering.** Finally, all generated question-answer pairs are manually reviewed. This review verifies the accuracy of object recognition, the logical consistency of spatial descriptions, the quality of the associated masks, and checks for grammatical errors to ensure the reliability of the final dataset. This final filtering stage yields 30,830 high-quality question-answer-masks triples. Additionally, to accommodate the demand for coarse localization, we

convert the masks into bounding box annotations via mask-to-bbox [31].

### 3.2. Data Statistics

As detailed in Table 1, LaSeRS is a large-scale dataset comprising 40,396 high-quality masks. The dataset's annotations span four types: textual instructions, textual answers, segmentation masks, and bounding boxes for coarse localization. The test set consists of 1,900 held-out masks and is meticulously partitioned to evaluate performance across four critical dimensions: **Hierarchical Segmentation Granularity** (semantic, instance, and part-level), **Target Multiplicity** (single, multiple), **Reasoning Requirements** (explicit, implicit), and **Linguistic Variability** (short, long). Figure 3 summarizes the statistical properties of LaSeRS. Panel (a) shows the distribution across 122 object categories, highlighting our dataset's broad coverage. This ensures the QA pairs are not skewed towards specific categories and exhibit high diversity. Further details on the categories are provided in the Suppl. 7.6. Panel (b) presents a word cloud of the instruction vocabulary. Panel (c) illustrates the instruction length distribution, ranging from just a few words to over 80, ensuring linguistic variability. Finally, panel (d) highlights the distribution of mask sizes, with a significant scale range from small, fine-grained parts to large regions exceeding 80% of the image area.

## 4. SegEarth-R2

To address the challenges of language-guided segmentation in RS, we introduce SegEarth-R2, a framework designed for precise, language-driven segmentation in RS images. As

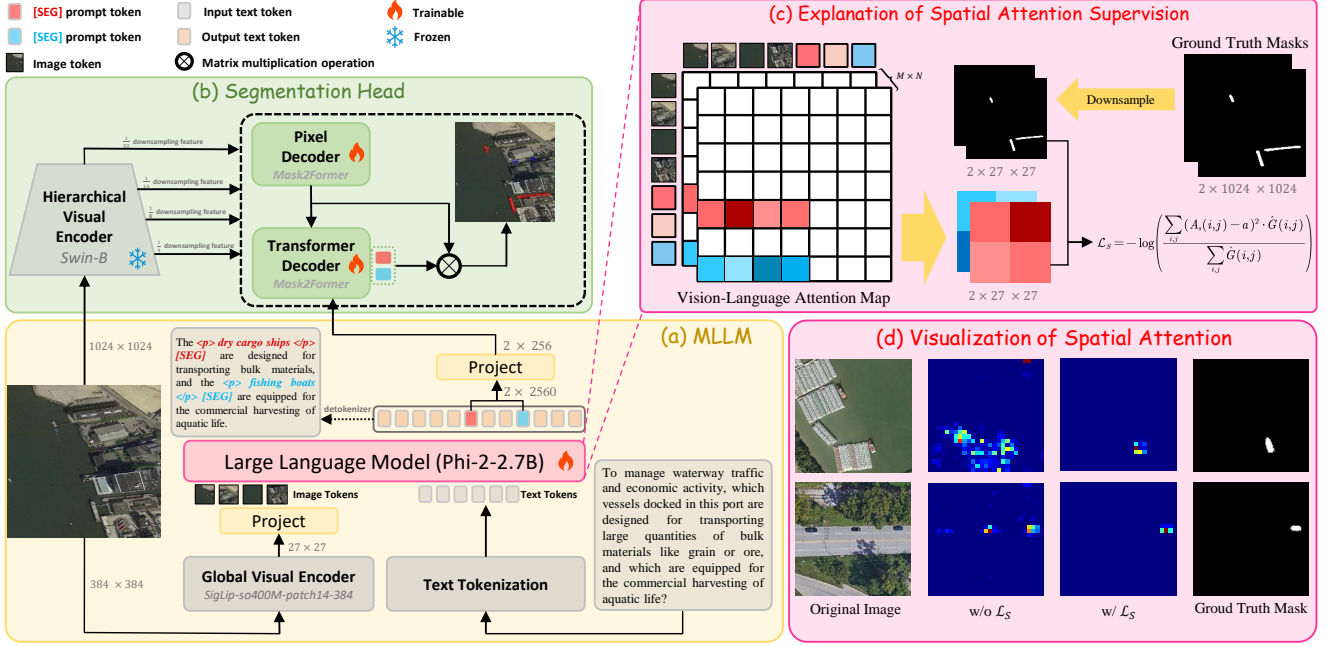


Figure 4. The overall architecture of SegEarth-R2. (a) is an MLLM for interpreting the image and instruction, (b) is the segmentation head, which includes a hierarchical visual encoder for generating multi-scale image features, and two decoders for producing masks (mask decoders). (c) illustrates the formation process of the spatial attention supervision. (d) presents a visualization of the attention map from the 6th head of the 16th layer in the MLLM, with additional visual results in the Suppl. 9.1

depicted in Figure 4, the model is composed of two primary components. The first is an MLLM that processes the input image and textual instruction to perform reasoning and generate a textual response. The second is a dedicated segmentation head that interprets the MLLM’s internal semantic representation, specifically the [SEG] token queries, to produce pixel-level masks. The performance of SegEarth-R2 relies on two key mechanisms corresponding to the above components: a spatial attention supervision mechanism applied to the model’s internal attention and a flexible and efficient segmentation query mechanism for mask generation, which are detailed in the following.

#### 4.1. Spatial Attention Supervision

A defining characteristic of RS images is the extreme variation in object scales, where targets can range from vast geographical features to entities spanning only a few pixels (*e.g.*, the small engine of an airplane). This presents a significant challenge for standard training paradigms. Supervision that relies solely on the final segmentation mask proves insufficient for instilling precise spatial awareness, as the learning signal becomes severely diluted when back-propagated to the network’s shallower layers. This dilution effect often leads to poor localization of small or complexly shaped objects, as visualized in Figure 4(d).

To counteract this, we introduce a spatial attention supervision mechanism, which provides direct supervisory sig-

nals to the model’s internal vision-language representations. Rather than inferring focus from the final output, our approach constitutes a direct intervention within the model’s reasoning pathway, compelling it to distinguish between foreground and background regions at the attention level. This process is illustrated in Figure 4(c).

This method operates on the attention maps originating from the [SEG] token to the image patch tokens within the MLLM’s transformer layers. Let  $A_{(m,n)} \in \mathbb{R}^{d \times d}$  denote the attention map for the  $n$ -th head in the  $m$ -th transformer block, where the model has a total of  $M$  blocks and  $N$  heads per block,  $d \times d$  represents the spatial dimensions of the image feature grid to which attention is applied. We then aggregate these individual maps into a unified attention grid by averaging them across all layers and heads, *i.e.*,  $A_S = \frac{1}{MN} \sum_{m=1}^M \sum_{n=1}^N A_{(m,n)}$ . Using a downsampled version of the ground truth mask,  $\hat{G} \in \{0, 1\}^{d \times d}$ , we calculate the average attention score,  $a$ , across all background regions:

$$a = \frac{\sum_{i,j} A_S(i,j) \cdot (1 - \hat{G}(i,j))}{\sum_{i,j} (1 - \hat{G}(i,j))}$$

where  $A_S(i,j)$  and  $\hat{G}(i,j)$  represent the  $i$ -th row and  $j$ -th column of the corresponding tensors.

The spatial attention supervision loss,  $\mathcal{L}_S$ , is then formulated to enforce a maximal separation between the attention

scores on the foreground regions and the calculated background average  $a$ :

$$\mathcal{L}_S = -\log \left( \frac{\sum_{i,j} (A_S(i,j) - a)^2 \cdot \hat{G}(i,j)}{\sum_{i,j} \hat{G}(i,j)} \right)$$

By maximizing the dissimilarity, this loss directly encourages the model to sharpen its focus specifically on the target area. This provides a clear and localized learning signal to the intermediate layers, substantially improving the model’s overall ability to ground and segment challenging objects with remarkable high fidelity.

## 4.2. Segmentation Query Mechanism

Previous approaches, such as InstructSeg [62], rely on a cumbersome “propose-then-select” strategy. They first generate a large pool of candidate masks (*e.g.*, 100) and are subsequently plagued by a redundant and time-consuming matching process to filter for the desired output; this design is not only computationally inefficient but also inflexible. On the other hand, while SegEarth-R1’s [28] “instruction-as-query” method offers simplicity, it is inherently limited by its assumption of a single target per instruction. This naive one-to-one mapping makes it fundamentally unsuitable for complex, multi-target scenarios.

As illustrated in Figure 4, to handle multi-target scenarios, we adopt the approach from LISA [19] by introducing a special [SEG] token. The model learns to dynamically output multiple [SEG] tokens based on the instruction’s context (*e.g.* “*In this area, we should stay away from the large, white < p > building < /p > [SEG] in the top-left corner, and run towards the large, < p > ground track field < /p > [SEG] to wait for rescue.*”), which then function as individual segmentation queries. Our architecture is composed of a Hierarchical Visual Encoder, *i.e.*, the Swin-B [38] which extracts multi-level image features. These features are then processed by a Pixel Decoder and a Transformer Decoder; we note that both of these modules adopt the identical architecture from Mask2Former [4]. The Pixel Decoder fuses the hierarchical features from the Swin-B, and the Transformer Decoder utilizes the [SEG] token queries to interact with these fused features, generating the final masks. This flexible and efficient segmentation query mechanism not only evades the redundant matching of “propose-then-select” methods but also capably handles the complex multi-target scenarios where “instruction-as-query” methods fail.

## 5. Experiment

### 5.1. Implementation Details

**Training objectives.** We train SegEarth-R2 with a unified loss function  $\mathcal{L}$ , which is the weighted sum of four distinct

components:

$$\mathcal{L} = \mathcal{L}_t + \mathcal{L}_b + \mathcal{L}_d + \lambda_S \mathcal{L}_S$$

Here,  $\mathcal{L}_t$  is the standard autoregressive cross-entropy loss for text generation. For mask supervision, we combine the per-pixel binary cross-entropy loss  $\mathcal{L}_b$  and DICE loss  $\mathcal{L}_d$ , while  $\mathcal{L}_S$  denotes the spatial attention supervision, which provides direct supervision on the model’s internal attention and is controlled by the coefficient  $\lambda_S$ .

**Experiment Settings.** We use the pre-trained lightweight MLLM Miphya-3B [80] as our base model. Following SegEarth-R1 [28], we use Swin-B [38] as the hierarchical visual encoder and the mask decoder from Mask2Former [4]. Furthermore, to conserve GPU memory, we keep all Visual Encoders frozen and employ LoRA with a rank of 8 to fine-tune the LLM, while the smaller Pixel Decoder and Transformer Decoder components are fully fine-tuned. More training details can be found in Suppl. 8.1.

**Metrics.** We use gIoU and cIoU as evaluation metrics, following prior studies [19, 63].

## 5.2. Main Results

As shown in Table 2, we conduct a comprehensive and fair evaluation on the LaSeRS benchmark, analyzing performance across four key dimensions.

**Hierarchical Segmentation Granularity.** We observe a consistent performance degradation across nearly all models as the segmentation granularity refines, *i.e.*, from the semantic-level, to the instance-level, and finally to the part-level, which often spans only a few pixels. This trend is expected, as finer granularities necessitate more precise model localization. Benefiting from our proposed spatial attention supervision mechanism, our model achieves the best performance across all granularities. This superiority is particularly pronounced at the challenging part-level, where our model surpasses the second-best method by a significant 20-point margin.

**Target Multiplicity.** For complex multi-target scenarios, we observe a significant performance degradation across most models. GeoPixel is a notable exception, which shows much less degradation, a result we attribute to the inherent strength of its 8B MLLM foundation [74]. We hypothesize that our model’s 3B size limits its performance in these complex multi-target scenarios. Even so, our model still secures the best performance on single-target tasks and the second-best on multi-target tasks, significantly outperforming other 7B and even 13B models.

**Reasoning Requirements.** All models exhibit significantly better performance on explicit instructions compared to implicit ones. This is an expected outcome, as implicit instructions, unlike their explicit counterparts, require the model to infer the target segmentation region by reasoning over the instruction’s context and its internal geographic knowledge.

Table 2. Performance comparison on LaSeRS. Baselines including LISA, PixelLM,  $M^2A$ , and GeoPixel are fine-tuned directly on LaSeRS. GLaMM-ft is pre-trained on large-scale natural image segmentation datasets before fine-tuning. Metrics are gIoU/cIoU. **Bold** and underlined indicate the best and second-best scores, respectively.

| Model            | Hierarchical Segmentation Granularity |                  |                  | Target Multiplicity |                   | Reasoning Requirements |                  | Linguistic Variability |                   | Avg.             |
|------------------|---------------------------------------|------------------|------------------|---------------------|-------------------|------------------------|------------------|------------------------|-------------------|------------------|
|                  | Semantic                              | Instance         | Part             | Single              | Multiple          | Explicit               | Implicit         | Short                  | Long              |                  |
| LISA-7B [19]     | 26.4/23.2                             | 20.5/25.0        | 16.1/11.6        | 37.3/32.2           | 18.2/22.4         | 27.1/24.3              | 21.5/25.6        | 34.1/27.8              | 38.4/33.9         | 26.6/25.1        |
| LISA-13B [19]    | 27.0/24.5                             | 22.3/25.6        | 17.7/13.1        | 38.4/34.2           | 19.9/23.5         | 27.1/25.5              | 22.6/25.8        | 35.2/28.0              | 38.4/34.3         | 27.6/26.1        |
| PixelLM-7B [48]  | 32.0/32.8                             | 26.6/30.0        | 13.2/16.5        | 44.3/40.4           | 20.2/23.5         | 25.0/23.1              | 23.9/21.9        | 41.6/38.9              | 37.1/34.5         | 29.3/29.1        |
| PixelLM-13B [48] | 31.6/34.0                             | 27.5/30.2        | 15.8/17.6        | 42.2/40.5           | 20.9/22.4         | 26.3/24.4              | 25.9/22.1        | 42.0/39.1              | 37.1/34.5         | 29.9/29.4        |
| GLaMM-ft-7B [46] | 44.8/47.9                             | 41.2/48.3        | 32.6/42.7        | 47.3/50.3           | 32.2/41.0         | 59.1/60.3              | 42.6/44.8        | 50.4/54.8              | 42.6/44.8         | 43.6/48.3        |
| $M^2A$ -7B [16]  | 30.1/33.0                             | 23.0/24.8        | 18.6/17.2        | 45.4/37.6           | 20.9/24.8         | 35.8/30.4              | 23.3/26.7        | 35.8/32.8              | 41.5/36.7         | 30.5/29.3        |
| GeoPixel-8B [50] | 51.4/57.2                             | 44.1/49.3        | 43.9/52.4        | 55.0/45.8           | <b>49.2/49.7</b>  | 66.5/61.3              | 41.1/58.3        | 51.1/59.3              | <b>51.4/63.2</b>  | 50.4/55.2        |
| SegEarth-R2-3B   | <b>60.2/71.8</b>                      | <b>65.4/70.3</b> | <b>64.8/68.3</b> | <b>55.1/69.2</b>    | 38.3/ <b>56.2</b> | <b>78.4/80.4</b>       | <b>42.8/59.7</b> | <b>60.2/69.9</b>       | 50.1/ <b>65.7</b> | <b>57.2/67.9</b> |

Table 3. Performance comparison on three RS referring segmentation benchmarks. To ensure a fair comparison, our results are obtained by training separately on each of the three training set. The metric is gIoU.

| Method                          | Pub      | RRSIS-D     |             | RefSegRS    |             | RISBench    |             | Avg. |
|---------------------------------|----------|-------------|-------------|-------------|-------------|-------------|-------------|------|
|                                 |          | val         | test        | val         | test        | val         | test        |      |
| <i>Segmentation Specialists</i> |          |             |             |             |             |             |             |      |
| CMPC+ [35]                      | TPAMI'21 | 51.4        | 50.2        | 47.1        | 43.7        | 45.8        | 46.7        |      |
| RIS-DMMI [13]                   | CVPR'23  | 60.7        | 60.1        | 65.7        | 52.2        | <u>62.6</u> | <u>63.9</u> |      |
| LAVT [67]                       | CVPR'22  | 61.5        | 61.0        | 61.5        | 47.4        | 60.5        | 61.9        |      |
| RMSIN [36]                      | CVPR'24  | 65.1        | 64.2        | 73.8        | 62.6        | 61.8        | 63.1        |      |
| <i>MLLM based segmentation</i>  |          |             |             |             |             |             |             |      |
| LISA [19]                       | CVPR'24  | 27.8        | 26.8        | -           | -           | -           | -           |      |
| PixelLM [48]                    | CVPR'24  | 33.9        | 31.7        | -           | -           | -           | -           |      |
| GeoGround [79]                  | arXiv'24 | 61.1        | 60.5        | -           | -           | -           | -           |      |
| GeoPixel [50]                   | ICML'25  | <u>68.0</u> | <u>67.3</u> | -           | -           | -           | -           |      |
| SegEarth-R1 [28]                | arXiv'25 | 67.6        | 66.4        | <u>82.2</u> | <u>72.5</u> | -           | -           |      |
| Text4Seg++ [22]                 | arXiv'25 | 64.1        | 62.8        | -           | -           | -           | -           |      |
| SegEarth-R2                     |          | <b>68.8</b> | <b>67.9</b> | <b>84.4</b> | <b>74.8</b> | <b>69.8</b> | <b>70.5</b> |      |

Table 4. Performance comparison on RS reasoning segmentation benchmark: EarthReason [28]. Our model is trained solely on the EarthReason training set.

| Method              | LLM          | Val         |             | Test        |             | Avg.        |
|---------------------|--------------|-------------|-------------|-------------|-------------|-------------|
|                     |              | gIoU        | cIoU        | gIoU        | cIoU        |             |
| LISA [19]           | Vicuna-7B    | 61.0        | 57.4        | 60.9        | 59.1        | 59.6        |
| PixelLM [48]        | Vicuna-7B    | 57.9        | 57.8        | 60.0        | 59.2        | 58.7        |
| SegEarth-R1 [28]    | Phi-1.5-1.3B | 68.6        | 64.1        | 70.8        | 68.3        | 68.0        |
| RemoteReasoner [70] | Qwen2.5-7B   | 69.0        | 67.8        | 71.0        | <u>69.1</u> | 69.2        |
| Text4Seg++ [22]     | Qwen2-7B     | <u>71.9</u> | <b>69.8</b> | <u>73.0</u> | 65.6        | <u>70.1</u> |
| SegEarth-R2-3B      | Phi-2-2.7B   | <b>72.3</b> | <u>68.1</u> | <b>73.5</b> | <b>69.5</b> | <b>70.9</b> |

Notably, our model achieves excellent performance on both explicit and implicit instructions.

**Linguistic Variability.** Regarding linguistic variability, we observe an interesting phenomenon: models respond differently to instruction length. Specifically, LISA,  $M^2A$ , and GeoPixel excel at processing long, detailed instructions. In contrast, PixelLM, GLaMM, and SegEarth-R2 show more prominent performance on short, concise instructions. We hypothesize this divergence stems from fundamental differences in their model architectures. Notably, SegEarth-R2

demonstrates strong robustness, achieving superior performance on both instruction types.

**Overall.** With only 3B parameters, SegEarth-R2 significantly outperforms all other models on average, a result that showcases the superiority of our architecture. More qualitative results can be found in the Suppl. 10.1.

### 5.3. Results on Existing Benchmarks

To ensure SegEarth-R2’s effectiveness is not limited to our proposed benchmark, we assess its generalization capabilities on established public datasets. For fair comparison, the model was trained separately on each benchmark’s official training split.

**RS Referring Segmentation.** We evaluate on three referring segmentation benchmarks: RRSIS-D [36], RefSegRS [72], and RISBench [9]. As shown in Table 3, SegEarth-R2 demonstrates strong cross-dataset generalization. On the RRSIS-D dataset, it outperforms the powerful 8B model, GeoPixel. On RefSegRS, SegEarth-R2 surpasses the previous state-of-the-art method by over 2 points. Furthermore, our model achieves the best performance on the larger-scale RISBench dataset. Qualitative results are provided in the Suppl. 10.2.

**RS Reasoning Segmentation.** On the more challenging EarthReason [28] benchmark for implicit reasoning segmentation in RS, as shown in Table 4, our model achieves an average score of 70.9, outperforming the previous state-of-the-art, Text4Seg++ (70.1), which represents masks using text. It also surpasses RemoteReasoner, a method exploring reinforcement learning for RS reasoning segmentation, demonstrating the superiority of our architecture in processing complex implicit instructions. Qualitative results are provided in Suppl. 10.3.

### 5.4. Ablation Study

We conduct thorough ablation studies on our proposed spatial attention supervision ( $\mathcal{L}_S$ ) and the adopted segmentation query mechanism. Furthermore, we investigate different combinations of the Segmentation Head (shown in Fig.

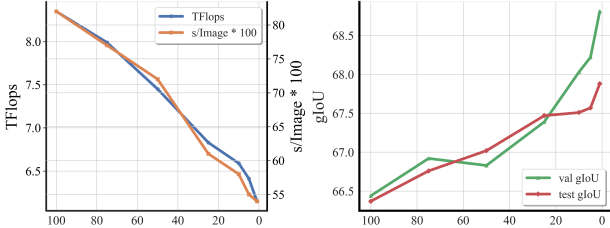


Figure 5. The left figure shows that as the number of segmentation queries decreases, both computational cost (TFLOPs) and inference time are correspondingly reduced. The right figure illustrates that this reduction in queries leads to a gradual increase in gIoU scores on the RRSIS-D validation and test sets.

Table 5. Ablation experiment on  $\lambda_S$ , which controls the strength of the spatial attention supervision in the MLLM inner layers. The metric is gIoU.

| $\lambda_S$ | $\mathcal{L}_S$ | RRSIS-D     |             | RefSegRS    |             | EarthReason |             |
|-------------|-----------------|-------------|-------------|-------------|-------------|-------------|-------------|
|             |                 | val         | test        | val         | test        | val         | test        |
| 0           | $\times$        | 68.5        | 66.6        | 81.1        | 70.4        | 72.2        | 72.9        |
| 0.1         | $\checkmark$    | 68.1        | 67.3        | 82.2        | 71.1        | 70.1        | 71.8        |
| 0.05        | $\checkmark$    | 68.6        | 67.7        | 82.2        | 71.7        | 72.1        | 73.0        |
| 0.01        | $\checkmark$    | <b>68.8</b> | <b>67.9</b> | <b>82.4</b> | <b>71.8</b> | <b>72.3</b> | <b>73.5</b> |

Table 6. The comparison between different combination of segmentation head. ViT-H: Vision Transformer Huge, Swin-B: Swin Transformer Base, SAM: Segment Anything Model, M2F: Mask2Former. The metric is gIoU.

| Mask Decoder | Visual Encoder | EarthReason |             | RefSegRS    |             |
|--------------|----------------|-------------|-------------|-------------|-------------|
|              |                | val         | test        | val         | test        |
| SAM [17]     | ViT-H [53]     | 62.7        | 65.4        | 73.9        | 60.3        |
| SAM 2 [47]   | ViT-H [53]     | 64.3        | 64.9        | 74.2        | 64.2        |
| M2F [4]      | Swin-B [38]    | <b>72.3</b> | <b>73.5</b> | <b>82.4</b> | <b>71.8</b> |

ure 4) to demonstrate the superiority of our architecture.

**Spatial Attention Supervision Effect.** The coefficient  $\lambda_S$  controls the weight of spatial attention supervision  $\mathcal{L}_S$ . We perform an ablation study on  $\lambda_S$ , and the results are shown in Table 5. As shown, setting  $\lambda_S = 0$ , which removes this supervision, results in the worst performance, highlighting the necessity of spatial attention guidance. However, we observe that excessively large values of  $\lambda_S$  (e.g., 0.1 or 0.05) degrade performance. We hypothesize this occurs because overly constraining the MLLM’s internal attention impairs its reasoning abilities. We find that  $\lambda_S = 0.01$  strikes the optimal balance and adopt it as our final setting. Notably, this value represents the best result in our discrete ablation set; further fine-grained searches could potentially yield a marginally better optimum. The improvement from this supervision is small on the EarthReason benchmark, which we attribute to its limited scale variation and the predominance of large objects.

**Segmentation Query Mechanism Effect.** Previous works [56, 61, 62, 77] use 100 segmentation queries to gen-

erate candidate masks and select the best one via a matching algorithm. Our experiments show that this approach is both redundant and inefficient. Specifically, we evaluate the number of segmentation queries  $k$ , using values  $k \in \{100, 75, 50, 25, 10, 3, 1\}$ . When  $k > 1$ , the single [SEG] token is replaced by a sequence of  $k$  independent query tokens, [SEG1] [SEG2] ... [SEG $k$ ]. The model correspondingly generates  $k$  proposal masks, and a matching algorithm [4] is then employed to select the optimal mask from the  $k$  candidates. When  $k = 1$ , the model generates a single mask that is directly used as the final output, bypassing the matching process. As shown in Figure 5, reducing the number of segmentation queries from 100 to just 1 results in a 34.1% reduction in inference time (from 0.82 to 0.54 s/image) and a 27.4% decrease in computational cost (from 8.4 to 6.1 TFLOPs), while also improving the gIoU score on the RRSIS-D [36] validation set by +2.4 points (66.4  $\rightarrow$  68.8) and on the test set by +1.6 points (66.3  $\rightarrow$  67.9). Visual analysis is provided in the Suppl. 9.2.

**Combination of Segmentation Head Analysis.** We substitute the Pixel Decoder and Transformer Decoder module (Figure 4) with SAM or SAM2 decoder. Concurrently, the Hierarchical Visual Encoder (Swin-B) is also replaced with the corresponding ViT-H backbone. Table 6 shows the results on EarthReason [28] and RefSegRS [72]. The combination of a multi-scale Swin Transformer and a Mask2Former decoder significantly outperforms architectures based on ViT-H and SAM or SAM2 decoder. This confirms that a hierarchical vision backbone, which is adept at capturing features across a wide range of scales, is better suited for the unique challenges of RS images compared to monolithic vision transformers. Our architectural choices are thus empirically validated as optimal for RS domain.

## 6. Conclusion

In this work, we explore comprehensive language-guided segmentation in RS. To advance this task, we present LaSeRS, the first large-scale benchmark designed to systematically investigate four key dimensions of language-guided segmentation: hierarchical granularity, target multiplicity, complex reasoning, and linguistic variability. This benchmark provides the community with a valuable resource to drive progress beyond simple, single-target instructions. To address the challenges of this benchmark, we propose SegEarth-R2, an effective and efficient MLLM architecture. Our evaluations show that SegEarth-R2 not only excels on the challenges posed by LaSeRS but also establishes a new SOTA across a range of established referring and reasoning segmentation benchmarks. Ultimately, we hope this work catalyzes a paradigm shift in the RS community, moving beyond parsing simple, single-target instructions toward developing comprehensive, unified language-guided segmentation.

## References

[1] Xiao An, Jiaxing Sun, Zihan Gui, and Wei He. Choice: Benchmarking the remote sensing capabilities of large vision-language models. *arXiv preprint arXiv:2411.18145*, 2024. 2

[2] Yakoub Bazi, Laila Bashmal, Mohamad Mahmoud Al Rahhal, Riccardo Ricci, and Farid Melgani. Rs-llava: A large vision-language model for joint captioning and question answering in remote sensing imagery. *Remote Sensing*, 16(9): 1477, 2024. 2

[3] Zhenyuan Chen, Chenxi Wang, Ningyu Zhang, and Feng Zhang. Rsc: A large-scale remote sensing change caption dataset for disaster events. *arXiv preprint arXiv:2509.01907*, 2025. 2

[4] Bowen Cheng, Ishan Misra, Alexander G Schwing, Alexander Kirillov, and Rohit Girdhar. Masked-attention mask transformer for universal image segmentation. In *Proceedings of the IEEE/CVF Conference on Computer Vision and Pattern Recognition*, pages 1290–1299, 2022. 3, 6, 8

[5] Gheorghe Comanici, Eric Bieber, Mike Schaekermann, Ice Pasupat, Noveen Sachdeva, Inderjit Dhillon, Marcel Blistein, Ori Ram, Dan Zhang, Evan Rosen, et al. Gemini 2.5: Pushing the frontier with advanced reasoning, multimodality, long context, and next generation agentic capabilities. *arXiv preprint arXiv:2507.06261*, 2025. 3

[6] Wenliang Dai, Junnan Li, Dongxu Li, Anthony Tiong, Junqi Zhao, Weisheng Wang, Boyang Li, Pascale N Fung, and Steven Hoi. Instructclip: Towards general-purpose vision-language models with instruction tuning. *Advances in neural information processing systems*, 36:49250–49267, 2023. 2

[7] Muhammad Sohail Danish, Muhammad Akhtar Munir, Syed Roshaan Ali Shah, Kartik Kuckreja, Fahad Shahbaz Khan, Paolo Fraccaro, Alexandre Lacoste, and Salman Khan. Geobench-vlm: Benchmarking vision-language models for geospatial tasks. In *Proceedings of the IEEE/CVF International Conference on Computer Vision (ICCV)*, 2025. 2

[8] Henghui Ding, Chang Liu, Suchen Wang, and Xudong Jiang. Vision-language transformer and query generation for referring segmentation. In *Proceedings of the IEEE/CVF international conference on computer vision*, pages 16321–16330, 2021. 3

[9] Zhe Dong, Yuzhe Sun, Tianzhu Liu, Wangmeng Zuo, and Yanfeng Gu. Cross-modal bidirectional interaction model for referring remote sensing image segmentation. *arXiv preprint arXiv:2410.08613*, 2024. 2, 3, 7

[10] Qiushan Guo, Shalini De Mello, Hongxu Yin, Wonmin Byeon, Ka Chun Cheung, Yizhou Yu, Ping Luo, and Sifei Liu. Regionopt: Towards region understanding vision language model. In *Proceedings of the IEEE/CVF Conference on Computer Vision and Pattern Recognition*, pages 13796–13806, 2024. 2

[11] Yue Han, Jiangning Zhang, Junwei Zhu, Runze Hou, Xiaozhong Ji, Chuming Lin, Xiaobin Hu, Zhucun Xue, and Yong Liu. Groundingface: Fine-grained face understanding via pixel grounding multimodal large language model. In *Proceedings of the Computer Vision and Pattern Recognition Conference*, pages 3942–3951, 2025. 3

[12] Rui Hu, Lianghui Zhu, Yuxuan Zhang, Tianheng Cheng, Lei Liu, Heng Liu, Longjin Ran, Xiaoxin Chen, Wenyu Liu, and Xinggang Wang. Groundingsuite: Measuring complex multi-granular pixel grounding. *arXiv preprint arXiv:2503.10596*, 2025. 3

[13] Yutao Hu, Qixiong Wang, Wenqi Shao, Enze Xie, Zhenguo Li, Jungong Han, and Ping Luo. Beyond one-to-one: Rethinking the referring image segmentation. In *Proceedings of the IEEE/CVF International Conference on Computer Vision*, pages 4067–4077, 2023. 7

[14] Yuan Hu, Jianlong Yuan, Congcong Wen, Xiaonan Lu, Yu Liu, and Xiang Li. Rsgpt: A remote sensing vision language model and benchmark. *ISPRS Journal of Photogrammetry and Remote Sensing*, 224:272–286, 2025. 2

[15] Jeremy Andrew Irvin, Emily Ruoyu Liu, Joyce Chui Chen, Ines Dormoy, Jinyoung Kim, Samar Khanna, Zhuo Zheng, and Stefano Ermon. Teochat: A large vision-language assistant for temporal earth observation data. In *International Conference on Learning Representations*, 2025. 2

[16] Donggon Jang, Yucheol Cho, Suin Lee, Taehyeon Kim, and Daeshik Kim. MMR: A large-scale benchmark dataset for multi-target and multi-granularity reasoning segmentation. In *The Thirteenth International Conference on Learning Representations*, 2025. 3, 7

[17] Alexander Kirillov, Eric Mintun, Nikhila Ravi, Hanzi Mao, Chloe Rolland, Laura Gustafson, Tete Xiao, Spencer Whitehead, Alexander C Berg, Wan-Yen Lo, et al. Segment anything. In *Proceedings of the IEEE/CVF international conference on computer vision*, pages 4015–4026, 2023. 3, 8

[18] Kartik Kuckreja, Muhammad Sohail Danish, Muzammal Naseer, Abhijit Das, Salman Khan, and Fahad Shahbaz Khan. Geochat: Grounded large vision-language model for remote sensing. In *Proceedings of the IEEE/CVF Conference on Computer Vision and Pattern Recognition*, pages 27831–27840, 2024. 2

[19] Xin Lai, Zhuotao Tian, Yukang Chen, Yanwei Li, Yuhui Yuan, Shu Liu, and Jiaya Jia. Lisa: Reasoning segmentation via large language model. In *Proceedings of the IEEE/CVF Conference on Computer Vision and Pattern Recognition*, pages 9579–9589, 2024. 2, 3, 6, 7

[20] Mengcheng Lan, Chaofeng Chen, Yue Zhou, Jiaxing Xu, Yiping Ke, Xinjiang Wang, Litong Feng, and Wayne Zhang. Text4seg: Reimagining image segmentation as text generation. *arXiv preprint arXiv:2410.09855*, 2024. 3

[21] Mengcheng Lan, Chaofeng Chen, Jiaxing Xu, Zongrui Li, Yiping Ke, Xudong Jiang, Yingchen Yu, Yunqing Zhao, and Song Bai. Text4seg++: Advancing image segmentation via generative language modeling. *arXiv preprint arXiv:2509.06321*, 2025. 3

[22] Mengcheng Lan, Chaofeng Chen, Jiaxing Xu, Zongrui Li, Yiping Ke, Xudong Jiang, Yingchen Yu, Yunqing Zhao, and Song Bai. Text4seg++: Advancing image segmentation via generative language modeling, 2025. 7

[23] Sen Lei, Xinyu Xiao, Tianlin Zhang, Heng-Chao Li, Zhenwei Shi, and Qing Zhu. Exploring fine-grained image-text alignment for referring remote sensing image segmentation. *IEEE Transactions on Geoscience and Remote Sensing*, 2024. 2

[24] Bo Li, Yuanhan Zhang, Dong Guo, Renrui Zhang, Feng Li, Hao Zhang, Kaichen Zhang, Peiyuan Zhang, Yanwei Li, Zi-wei Liu, et al. Llava-onevision: Easy visual task transfer. *arXiv preprint arXiv:2408.03326*, 2024. 2

[25] Kaiyu Li, Xiangyong Cao, Yupeng Deng, Chao Pang, Zepeng Xin, Deyu Meng, and Zhi Wang. Dynamicearth: How far are we from open-vocabulary change detection? *arXiv preprint arXiv:2501.12931*, 2025. 2

[26] Kaiyu Li, Xiangyong Cao, Ruixun Liu, Shihong Wang, Zixuan Jiang, Zhi Wang, and Deyu Meng. Annotation-free open-vocabulary segmentation for remote-sensing images. *arXiv preprint arXiv:2508.18067*, 2025. 2

[27] Kaiyu Li, Ruixun Liu, Xiangyong Cao, Xueru Bai, Feng Zhou, Deyu Meng, and Zhi Wang. Segearth-ov: Towards training-free open-vocabulary segmentation for remote sensing images. In *Proceedings of the Computer Vision and Pattern Recognition Conference*, pages 10545–10556, 2025. 2

[28] Kaiyu Li, Zepeng Xin, Li Pang, Chao Pang, Yupeng Deng, Jing Yao, Guisong Xia, Deyu Meng, Zhi Wang, and Xiangyong Cao. Segearth-r1: Geospatial pixel reasoning via large language model. *arXiv preprint arXiv:2504.09644*, 2025. 2, 3, 6, 7, 8, 1

[29] Xiang Li, Jian Ding, and Mohamed Elhoseiny. Vrsbench: A versatile vision-language benchmark dataset for remote sensing image understanding. In *The Thirty-eight Conference on Neural Information Processing Systems Datasets and Benchmarks Track*. 2

[30] Zhenshi Li, Dilxat Muhtar, Feng Gu, Yanglangxing He, Xueliang Zhang, Pengfeng Xiao, Guangjun He, and Xiaoxiang Zhu. Lhrs-bot-nova: Improved multimodal large language model for remote sensing vision-language interpretation. *ISPRS Journal of Photogrammetry and Remote Sensing*, 227:539–550, 2025. 2

[31] Fan Liu, Delong Chen, Zhangqiyun Guan, Xiaocong Zhou, Jiale Zhu, Qiaolin Ye, Liyong Fu, and Jun Zhou. Remoteclip: A vision language foundation model for remote sensing. *IEEE Transactions on Geoscience and Remote Sensing*, 62:1–16, 2024. 4

[32] Haotian Liu, Chunyuan Li, Qingyang Wu, and Yong Jae Lee. Visual instruction tuning. *Advances in neural information processing systems*, 36:34892–34916, 2023. 2

[33] Haotian Liu, Chunyuan Li, Yuheng Li, and Yong Jae Lee. Improved baselines with visual instruction tuning. In *Proceedings of the IEEE/CVF conference on computer vision and pattern recognition*, pages 26296–26306, 2024. 2

[34] Jiang Liu, Hui Ding, Zhaowei Cai, Yuting Zhang, Ravi Kumar Satzoda, Vijay Mahadevan, and R Manmatha. Polyformer: Referring image segmentation as sequential polygon generation. In *Proceedings of the IEEE/CVF conference on computer vision and pattern recognition*, pages 18653–18663, 2023. 3

[35] Si Liu, Tianrui Hui, Shaofei Huang, Yunchao Wei, Bo Li, and Guanbin Li. Cross-modal progressive comprehension for referring segmentation. *IEEE Transactions on Pattern Analysis and Machine Intelligence*, 44(9):4761–4775, 2021. 7

[36] Sihan Liu, Yiwei Ma, Xiaoqing Zhang, Haowei Wang, Jiayi Ji, Xiaoshuai Sun, and Rongrong Ji. Rotated multi-scale interaction network for referring remote sensing image segmentation. In *Proceedings of the IEEE/CVF Conference on Computer Vision and Pattern Recognition*, pages 26658–26668, 2024. 2, 3, 7, 8

[37] Xu Liu and Zhouhui Lian. Rsunivlm: A unified vision language model for remote sensing via granularity-oriented mixture of experts. *arXiv preprint arXiv:2412.05679*, 2024. 3

[38] Ze Liu, Yutong Lin, Yue Cao, Han Hu, Yixuan Wei, Zheng Zhang, Stephen Lin, and Baining Guo. Swin transformer: Hierarchical vision transformer using shifted windows. In *Proceedings of the IEEE/CVF international conference on computer vision*, pages 10012–10022, 2021. 6, 8

[39] Siqi Lu, Junlin Guo, James R Zimmer-Dauphinee, Jordan M Nieuwsma, Xiao Wang, Steven A Wernke, Yuankai Huo, et al. Vision foundation models in remote sensing: A survey. *IEEE Geoscience and Remote Sensing Magazine*, 2025. 2

[40] Xianzhi Ma, Jianhui Li, Changhua Pei, and Hao Liu. Geomag: A vision-language model for pixel-level fine-grained remote sensing image parsing. *arXiv preprint arXiv:2507.05887*, 2025. 3

[41] Ruizhe Ou, Yuan Hu, Fan Zhang, Jiaxin Chen, and Yu Liu. Geopix: A multimodal large language model for pixel-level image understanding in remote sensing. *IEEE Geoscience and Remote Sensing Magazine*, 2025. 2, 3

[42] Chao Pang, Jiang Wu, Jiayu Li, Yi Liu, Jiaxing Sun, Weijia Li, Xingxing Weng, Shuai Wang, Litong Feng, Gui-Song Xia, et al. H2rsvlm: Towards helpful and honest remote sensing large vision language model. *CoRR*, 2024. 2

[43] Chao Pang, Xingxing Weng, Jiang Wu, Jiayu Li, Yi Liu, Jiaxing Sun, Weijia Li, Shuai Wang, Litong Feng, Gui-Song Xia, et al. Vhm: Versatile and honest vision language model for remote sensing image analysis. In *Proceedings of the AAAI Conference on Artificial Intelligence*, pages 6381–6388, 2025. 2

[44] Jerome Quenum, Wen-Han Hsieh, Tsung-Han Wu, Ritwik Gupta, Trevor Darrell, and David M Chan. Lisat: Language-instructed segmentation assistant for satellite imagery. *arXiv preprint arXiv:2505.02829*, 2025. 3

[45] Maryam Rahnemoonfar, Tashnim Chowdhury, Argho Sarkar, Debrat Varshney, Masoud Yari, and Robin Robertson Murphy. Floodnet: A high resolution aerial imagery dataset for post flood scene understanding. *IEEE Access*, 9:89644–89654, 2021. 2

[46] Hanoona Rasheed, Muhammad Maaz, Sahal Shaji, Abdelrahman Shaker, Salman Khan, Hisham Cholakkal, Rao M. Anwer, Eric Xing, Ming-Hsuan Yang, and Fahad S. Khan. Glamm: Pixel grounding large multimodal model. *The IEEE/CVF Conference on Computer Vision and Pattern Recognition*, 2024. 7

[47] Nikhila Ravi, Valentin Gabeur, Yuan-Ting Hu, Ronghang Hu, Chaitanya Ryali, Tengyu Ma, Haitham Khedr, Roman Rädle, Chloe Rolland, Laura Gustafson, et al. Sam 2: Segment anything in images and videos. *arXiv preprint arXiv:2408.00714*, 2024. 3, 8

[48] Zhongwei Ren, Zhicheng Huang, Yunchao Wei, Yao Zhao, Dongmei Fu, Jiashi Feng, and Xiaojie Jin. Pixellm: Pixel

reasoning with large multimodal model. In *Proceedings of the IEEE/CVF Conference on Computer Vision and Pattern Recognition*, pages 26374–26383, 2024. 3, 7

[49] Esther Rolf, Konstantin Klemmer, Caleb Robinson, and Hannah Kerner. Mission critical–satellite data is a distinct modality in machine learning. *arXiv preprint arXiv:2402.01444*, 2024. 2

[50] Akashah Shabbir, Mohammed Zumri, Mohammed Ben-namoun, Fahad S Khan, and Salman Khan. Geopixel: Pixel grounding large multimodal model in remote sensing. *arXiv preprint arXiv:2501.13925*, 2025. 2, 3, 7

[51] Yan Shu, Bin Ren, Zhitong Xiong, Danda Pani Paudel, Luc Van Gool, Begum Demir, Nicu Sebe, and Paolo Rota. Earthmind: Towards multi-granular and multi-sensor earth observation with large multimodal models. *arXiv preprint arXiv:2506.01667*, 2025. 3

[52] Sagar Soni, Akshay Dudhane, Hiyam Debary, Mustansar Fiaz, Muhammad Akhtar Munir, Muhammad Sohail Danish, Paolo Fraccaro, Campbell D Watson, Levente J Klein, Fahad Shahbaz Khan, et al. Earthdial: Turning multi-sensory earth observations to interactive dialogues. In *Proceedings of the Computer Vision and Pattern Recognition Conference*, pages 14303–14313, 2025. 2

[53] Ashish Vaswani, Noam Shazeer, Niki Parmar, Jakob Uszkoreit, Llion Jones, Aidan N Gomez, Łukasz Kaiser, and Illia Polosukhin. Attention is all you need. *Advances in neural information processing systems*, 30, 2017. 8

[54] Di Wang, Jing Zhang, Bo Du, Minqiang Xu, Lin Liu, Dacheng Tao, and Liangpei Zhang. Samrs: Scaling-up remote sensing segmentation dataset with segment anything model. In *Advances in Neural Information Processing Systems*, pages 8815–8827, 2023. 3

[55] Fengxiang Wang, Mingshuo Chen, Yueying Li, Di Wang, Haotian Wang, Zonghao Guo, Zefan Wang, Boqi Shan, Long Lan, Yulin Wang, et al. Geollava-8k: Scaling remote-sensing multimodal large language models to 8k resolution. *arXiv preprint arXiv:2505.21375*, 2025. 2

[56] Hao Wang, Limeng Qiao, Zequn Jie, Zhijian Huang, Chengjian Feng, Qingfang Zheng, Lin Ma, Xiangyuan Lan, and Xiaodan Liang. X-sam: From segment anything to any segmentation. *arXiv preprint arXiv:2508.04655*, 2025. 3, 8

[57] Junjue Wang, Zhuo Zheng, Zihang Chen, Ailong Ma, and Yanfei Zhong. Earthvqa: Towards queryable earth via relational reasoning-based remote sensing visual question answering. In *Proceedings of the AAAI conference on artificial intelligence*, pages 5481–5489, 2024. 3

[58] Junjue Wang, Weihao Xuan, Heli Qi, Zhihao Liu, Kunyi Liu, Yuhua Wu, Hongruixuan Chen, Jian Song, Junshi Xia, Zhuo Zheng, et al. Disasterm3: A remote sensing vision-language dataset for disaster damage assessment and response. *arXiv preprint arXiv:2505.21089*, 2025. 2

[59] Zhaoqing Wang, Yu Lu, Qiang Li, Xunqiang Tao, Yandong Guo, Mingming Gong, and Tongliang Liu. Cris: Clip-driven referring image segmentation. In *Proceedings of the IEEE/CVF conference on computer vision and pattern recognition*, pages 11686–11695, 2022. 3

[60] Cong Wei, Haoxian Tan, Yujie Zhong, Yujiu Yang, and Lin Ma. Lasagna: Language-based segmentation assistant for complex queries. *arXiv preprint arXiv:2404.08506*, 2024. 3

[61] Cong Wei, Yujie Zhong, Haoxian Tan, Yong Liu, Zheng Zhao, Jie Hu, and Yujiu Yang. Hyperseg: Towards universal visual segmentation with large language model. *arXiv preprint arXiv:2411.17606*, 2024. 3, 8

[62] Cong Wei, Yujie Zhong, Haoxian Tan, Yingsen Zeng, Yong Liu, Zheng Zhao, and Yujiu Yang. Instructseg: Unifying instructed visual segmentation with multi-modal large language models. *arXiv preprint arXiv:2412.14006*, 2024. 2, 3, 6, 8

[63] Chenyun Wu, Zhe Lin, Scott Cohen, Trung Bui, and Subhransu Maji. Phrasescut: Language-based image segmentation in the wild. In *Proceedings of the IEEE/CVF Conference on Computer Vision and Pattern Recognition*, pages 10216–10225, 2020. 6

[64] Zhuofan Xia, Dongchen Han, Yizeng Han, Xuran Pan, Shiji Song, and Gao Huang. Gsva: Generalized segmentation via multimodal large language models. In *Proceedings of the IEEE/CVF Conference on Computer Vision and Pattern Recognition*, pages 3858–3869, 2024. 3

[65] Wentao Xiang, Haoxian Tan, Yujie Zhong, Cong Wei, Dengjie Li, and Yujiu Yang. Advancing visual large language model for multi-granular versatile perception. In *Proceedings of the IEEE/CVF International Conference on Computer Vision*, pages 22153–22164, 2025. 3

[66] Cilin Yan, Haochen Wang, Shilin Yan, Xiaolong Jiang, Yao Hu, Guoliang Kang, Weidi Xie, and Efstratios Gavves. Visa: Reasoning video object segmentation via large language models. In *European Conference on Computer Vision*, pages 98–115. Springer, 2024. 3

[67] Zhao Yang, Jiaqi Wang, Yansong Tang, Kai Chen, Hengshuang Zhao, and Philip HS Torr. Lavt: Language-aware vision transformer for referring image segmentation. In *Proceedings of the IEEE/CVF conference on computer vision and pattern recognition*, pages 18155–18165, 2022. 3, 7

[68] Zhigang Yang, Huiguang Yao, Linmao Tian, Xuezhi Zhao, Qiang Li, and Qi Wang. A large-scale referring remote sensing image segmentation dataset and benchmark. *arXiv preprint arXiv:2506.03583*, 2025. 3

[69] Kelu Yao, Nuo Xu, Rong Yang, Yingying Xu, Zhuoyan Gao, Titinunt Kitrungrotsakul, Yi Ren, Pu Zhang, Jin Wang, Ning Wei, et al. Falcon: A remote sensing vision-language foundation model. *arXiv preprint arXiv:2503.11070*, 2025. 3

[70] Liang Yao, Fan Liu, Hongbo Lu, Chuanyi Zhang, Rui Min, Shengxiang Xu, Shimin Di, and Pai Peng. Remotereasoner: Towards unifying geospatial reasoning workflow. *arXiv preprint arXiv:2507.19280*, 2025. 3, 7

[71] Haobo Yuan, Xiangtai Li, Tao Zhang, Zilong Huang, Shilin Xu, Shunping Ji, Yunhai Tong, Lu Qi, Jiashi Feng, and Ming-Hsuan Yang. Sa2va: Marrying sam2 with llava for dense grounded understanding of images and videos. *arXiv preprint arXiv:2501.04001*, 2025. 3

[72] Zhenghang Yuan, Lichao Mou, Yuansheng Hua, and Xiao Xiang Zhu. Rrsis: Referring remote sensing image segmentation. *IEEE Transactions on Geoscience and Remote Sensing*, 2024. 2, 3, 7, 8

[73] Yang Zhan, Zhitong Xiong, and Yuan Yuan. Skyeyegpt: Unifying remote sensing vision-language tasks via instruction tuning with large language model. *ISPRS Journal of Photogrammetry and Remote Sensing*, 221:64–77, 2025. 2

[74] Pan Zhang, Xiaoyi Dong, Yuhang Zang, Yuhang Cao, Rui Qian, Lin Chen, Qipeng Guo, Haodong Duan, Bin Wang, Linke Ouyang, et al. Internlm-xcomposer-2.5: A versatile large vision language model supporting long-contextual input and output. *arXiv preprint arXiv:2407.03320*, 2024. 6

[75] Shilong Zhang, Peize Sun, Shoufa Chen, Min Xiao, Wenqi Shao, Wenwei Zhang, Yu Liu, Kai Chen, and Ping Luo. Gpt4roi: Instruction tuning large language model on region-of-interest. In *European conference on computer vision*, pages 52–70. Springer, 2024. 2

[76] Wei Zhang, Miaoxin Cai, Tong Zhang, Yin Zhuang, and Xuerui Mao. Earthgpt: A universal multi-modal large language model for multi-sensor image comprehension in remote sensing domain. *IEEE Transactions on Geoscience and Remote Sensing*, 2024. 2

[77] Zheng Zhang, Yeyao Ma, Enming Zhang, and Xiang Bai. Psalm: Pixelwise segmentation with large multi-modal model. In *European Conference on Computer Vision*, pages 74–91. Springer, 2024. 3, 8

[78] Zilun Zhang, Zian Guan, Tiancheng Zhao, Haozhan Shen, Tianyu Li, Yuxiang Cai, Zhonggen Su, Zhaojun Liu, Jianwei Yin, and Xiang Li. Geo-r1: Improving few-shot geospatial referring expression understanding with reinforcement fine-tuning. *arXiv preprint arXiv:2509.21976*, 2025. 3

[79] Yue Zhou, Mengcheng Lan, Xiang Li, Litong Feng, Yiping Ke, Xue Jiang, Qingyun Li, Xue Yang, and Wayne Zhang. Geoground: A unified large vision-language model for remote sensing visual grounding. *arXiv preprint arXiv:2411.11904*, 2024. 2, 3, 7

[80] Minjie Zhu, Yichen Zhu, Xin Liu, Ning Liu, Zhiyuan Xu, Chaomin Shen, Yaxin Peng, Zhicai Ou, Feifei Feng, and Jian Tang. Mipha: A comprehensive overhaul of multi-modal assistant with small language models. *arXiv preprint arXiv:2403.06199*, 2024. 6

[81] Yongshuo Zong, Qin Zhang, Dongsheng An, Zhihua Li, Xiang Xu, Linghan Xu, Zhuowen Tu, Yifan Xing, and Onkar Dabeer. Ground-v: Teaching vlms to ground complex instructions in pixels. In *Proceedings of the Computer Vision and Pattern Recognition Conference*, pages 24635–24645, 2025. 3

# SegEarth-R2: Towards Comprehensive Language-guided Segmentation for Remote Sensing Images

## Supplementary Material

### 7. More information of LaSeRS

#### 7.1. Definition of Four Dimensions of LaSeRS

**Hierarchical Granularity.** A primary challenge in RS arises from the vast and complex nature of the imagery. A single scene often contains a diverse array of objects at vastly different scales, from large-scale collections (e.g., “all indistinguishable vehicles densely parked in the parking lot”) to specific instances (e.g., “a cargo truck parked in the bottom left”). Consequently, language queries used to describe these scenes inherently exhibit hierarchical granularity. As shown in Figure 1, this hierarchical granularity can be categorized into conceptual and segmentation granularity. The first, hierarchical concept granularity, relates to the level of semantic abstraction in the query, requiring the model to understand a hierarchy from coarse categories (e.g., “airplane”) to fine-grained sub-classes (e.g., “Boeing 787”). This is particularly challenging in RS images due to noise, small objects, and the need for expert knowledge. The second, hierarchical segmentation granularity, dictates the spatial scope of the desired output mask, which operates at three distinct levels: semantic (e.g., “all tennis courts”), instance (e.g., “the rightmost tennis court”), and part (e.g., “the service area of the rightmost tennis court”).

**Target Multiplicity.** This challenge arises from queries that reference multiple objects simultaneously, testing a model’s ability to parse and ground complex instructions. This is illustrated by the target multiplicity and long query cases in Figure 1.

**Reasoning Requirements.** This challenge spans a spectrum from explicit to implicit reasoning [28]. Explicit queries relate to literal visual attributes (e.g., “a large ground track field”). In contrast, implicit queries require commonsense knowledge; for example, processing “an escape direction in case of an earthquake” requires the model to infer safety by identifying open areas and avoiding dense structures.

**Linguistic Variability.** As shown in Figure 1, this incorporates both concise and long, descriptive queries to evaluate model robustness to varying levels of linguistic detail.

#### 7.2. The Details of Masks Generation

As shown in Figure 2, we employ two distinct point prompting strategies to generate candidate masks. For global point prompts, we set a grid parameter  $R = C = 4$ , uniformly sampling an  $R \times C$  grid of 16 points across the square image to prompt the SAM. For local point prompts, we

first utilize the provided bbox annotation to crop the target region. Points are then sampled exclusively within this cropped area. Assuming the cropped region has a height of  $h$  and a width of  $w$ , the sampling grid dimensions  $(R, C)$  are determined by:

$$(R, C) = \begin{cases} \left(\left\lceil \frac{\max\{h,w\}}{\min\{h,w\}} \right\rceil + 1, 1\right), & \text{if } \frac{\max\{h,w\}}{\min\{h,w\}} \geq 2.5 \\ (4, 4), & \text{if } 1 \leq \frac{\max\{h,w\}}{\min\{h,w\}} < 2.5 \end{cases}$$

#### 7.3. The Details of Masks Filtering

In this section, we detail the automated mask filtering pipeline, which is visually depicted in Figure 2. This process is designed to programmatically curate the dataset by removing low-quality or erroneous annotations. We use the “airplane” category as an illustrative example to describe this multi-stage procedure.

First, we perform a coarse-grained sanity check based on object counts. We iterate through all samples and discard any instance where the number of discrete connected components in the binary mask does not precisely match the number of associated bounding boxes. This step effectively removes clear anomalies, such as fragmented masks (i.e., multiple components for one box) or improperly merged masks (i.e., one component for multiple boxes).

Second, from the pool of samples that pass this initial check, we establish a “gold standard” reference set. This set consists of 50 high-quality “airplane” masks that were manually selected and verified by human annotators. This reference set serves as the exemplar distribution from which we derive the target geometric profile for the category.

Third, we derive and apply a set of heuristic thresholds by statistically analyzing this “gold standard” set. We calculate the following geometric properties for the primary connected component of each of the 50 reference masks. All calculations are implemented using the OpenCV library.

- **Eccentricity:** Measures how much the shape of the mask deviates from a perfect circle.
- **Circularity:** Quantifies the “roundness” of the mask, defined as  $\frac{4\pi \cdot \text{Area}}{\text{Perimeter}^2}$ .
- **Solidity:** The ratio of the mask’s area to the area of its convex hull. This metric penalizes shapes with significant indentations.
- **Symmetry:** A custom metric defined to quantify the object’s expected bilateral symmetry.
- **Extent:** The ratio of the mask’s area to the area of its bounding box ( $\frac{\text{Mask Area}}{\text{Bbox Area}}$ ). This filters masks that are

overly sparse.

By calculating the distribution (*e.g.*, mean and standard deviation) of these properties across the reference set, we establish an “acceptable range” for each metric. Finally, these ranges are applied as a fine-grained filter to all remaining masks in the dataset. A mask is retained only if all its geometric properties fall within these predefined bounds.

#### 7.4. The Details of QAs Generation

In this section, we detail the QA generation process, as shown in Figure 2. Our methodology adapts based on the mask source, which falls into two categories: those with pre-existing category labels and those without.

For masks with category labels, we employ two prompts, Prompt 6 and Prompt 7. Simple adjustments to these prompts generate a diverse set of QA pairs, allowing us to control factors such as output length and implicit reasoning.

Conversely, for masks that lack category labels, we first perform a preliminary category generation step. We use Prompt 8 to assign a category label to the masked region. Once the label is obtained, we then proceed to generate the corresponding QA pairs using the methods described above.

To execute this entire generation pipeline, we utilize the Gemini-2.5-Pro model, which we selected for its exceptional instruction-following capabilities. To ensure a high degree of diversity in the generated questions, we set the temperature parameter to 1.0. Furthermore, we enable its chain-of-thought reasoning capabilities to maintain high fidelity and coherence in the output.

#### 7.5. The Details of QAs Filtering

The initial generation phases produced a raw dataset of approximately 40k QA pairs. To ensure the highest standards of quality and eliminate any generation artifacts, we implemented a rigorous, multi-stage manual validation process. This critical task was performed by a team of 15 domain experts, all with extensive experience in remote sensing and computer vision.

Each of the 40k QA pairs was meticulously inspected against a four-point quality rubric. A pair was only retained if it passed all four criteria:

- **Object recognition:** Verifying the accuracy of object category recognition in the image.
- **Spatial description and logical consistency of the question:** Ensuring the spatial and logical accuracy of the question’s description.
- **Mask quality:** Assessing if the annotated mask meets quality standards for precision and completeness.
- **Grammatical accuracy:** Checking for grammatical mistakes or inconsistencies in the text.

Pairs that failed any of these checks were discarded. Following this comprehensive review, we performed a final quality assurance pass that involved randomly sampling the

filtered set to verify the consistency and quality of the experts’ work.

This expert-driven curation process yielded our final dataset, comprising 30,830 high-quality QA pairs that, in total, correspond to over 40,000 validated object masks.

#### 7.6. Category List of LaSeRS

Table 7 illustrates the category distribution of the LaSeRS dataset. Our dataset includes not only general categories but also fine-grained concepts and part-level categories.

#### 7.7. More Examples of LaSeRS

Figures 9 and 10 show more examples of LaSeRS.

### 8. Experiment Setting Details

#### 8.1. Training Details

Table 8 presents the specific training hyperparameters of SegEarth-R2. Training and testing were conducted on an Nvidia A100 80GB GPU.

### 9. Visual Analysis

#### 9.1. Visual Analysis of Spatial Attention

Figure 12 shows additional visualizations of the spatial attention mechanism. It can be observed that our spatial attention supervision helps the model better localize complex or small objects.

#### 9.2. Visual Analysis of Segmentation Query

Figure 13, Figure 14, Figure 15 and Figure 16 show the ground truth mask, the mask selected by matching algorithm and the candidate masks when segmentation query number is set to 100. In many cases, the mask selected by the matching algorithm is not optimal, which leads to losses in both efficiency and performance. We set the segmentation query number to 1, and Figure 5 demonstrates the results. It can be observed that both efficiency and performance have been significantly improved.

### 10. Qualitative Results of SegEarth-R2

#### 10.1. LaSeRS

Figure 17 and Figure 10 show the qualitative results on the LaSeRS test set.

#### 10.2. RefSegRS, RRSIS-D, and RISBench

Figure 19, Figure 20, and Figure 21 show the qualitative results on the RefSegRS, RRSIS-D, and RISBench benchmarks, respectively.

#### 10.3. EarthReason

Figure 22 show the qualitative results on EarthReason benchmark.

Table 7. Comparison of dataset categories: LaSeRS contains 122 categories, encompassing general, fine-grained, and part-level classes, and covering a wide range of remote sensing scenes such as land cover, vehicles, and natural landscapes. In contrast, RefSegRS, RRSIS-D, RISBench, and EarthReason contain only a dozen to around twenty categories.

| Dataset          | Categories   |
|------------------|--|
| LaSeRS           | <p><b>General:</b> airplane, airport, airport runway, bare land, baseball diamond, baseball field, basketball court, beach, bridge, bridge road, building, bushes, canal, chimney, cooling tower, dam, expressway service area, expressway toll station, farmland, football field, golf field, grass, green strip, greenhouse, ground track field, harbor, helicopter, helipad, intersection, jet bridge, lake, large vehicle, overpass, parking lot, path, paved road, paved square, plane, playground, railway, river, road, round-about, sea, ship, slide, small car, small vehicle, soccer ball field, solar panel, sports field, stadium, storage tank, substation, swimming pool, tennis court, terminal, train station, tree, unimproved road, vehicle, volleyball court, water, white smoke, windmill.</p> <p><b>Fine-grained Concept:</b> B1-B boomer, a220, a321, a330, a350, arj21, boeing737, boeing747, boeing777, boeing787, bus, c919, cargo truck, container crane, dry cargo ship, dockside warehouse, dump truck, driveway, engineering ship, excavator, fishing boat, hangar, liquid cargo ship, motor-boat, passenger ship, tractor, trailer, truck tractor, tugboat, van, warship.</p> <p><b>Part:</b> airplane engine, bleachers, bow of ship, cargo hold, center circle, center line, center service line, cooling tower shell, cooling tower top opening, downstream, football net, fuselage, horizontal stabilizer, industrial pipeline, net, no man's land of tennis court, riverbank, service box, shipping container, stern of ship, tennis net, three-point line, upstream, wake, wing, zebra crossing.</p> |
| RefSegRS [72]    | <b>General:</b> road, vehicle, car, van, building, truck, trailer, bus, road marking, bikeway, sidewalk, tree, low vegetation, impervious surface.   |
| RRSIS-D [36]     | <b>General:</b> airplane, airport, golf field, expressway service area, baseball field, stadium, ground track field, storage tank, basketball court, chimney, tennis court, overpass, train station, ship, express toll station, dam, harbor, bridge, vehicle, windmill.   |
| RISBench [9]     | <b>General:</b> expressive service area, expressive toll station, ground track field, basketball court, container crane, roundabout, windmill, overpass, stadium, bridge, soccer ball field, baseball diamond, train station, golf field, airport, harbor, dam, ship, helipad, vehicle, chimney, airplane, helicopter, tennis court, storage tank, swimming pool.  |
| EarthReason [28] | <b>General:</b> storage tank, bridge, intersection, tennis court, baseball field, substation, pier, viaduct, wind turbine, church, airport runway, swimming pool, lake, airport helipad, dam, railway, basketball court, beach, greenhouse, roundabout, solar power plant, ground track field, wastewater plant, river, train station, stadium, island, factory.   |

Table 8. Hyper parameters of our model in the training.

| Parameters             | Value  |
|------------------------|--|
| Optimizer              | AdamW  |
| Learning Rate          | $1 \times 10^{-4}$                                       |
| Batch Size             | 4  |
| Training Steps         | 50,000   |
| Learning Rate Schedule | Cosine Decay   |
| Lora Rank              | 8  |
| Computation Precision  | bf16   |
| Weight Decay           | 0.0  |
| Warmup Ratio           | 0.03   |
| Image Size             | $1024 \times 1024$                                       |
| Image Processing       | Resize long edge to 1024 and padding short edge to 1024. |

## Prompt:

Assume you are an expert in interpreting remote sensing imagery. I will provide you with a remote sensing image with annotations, where the annotated area is a target region outlined in red. I will also provide the object category name corresponding to this region. Based on the natural and socio-economic environment in the image, generate one implicit reasoning question-answer pair. Follow these requirements strictly:

1. The question must not directly mention the object category name. It should be implicit, requiring reasoning to infer the object type of the target region.
2. Imagine a realistic scenario based on the image context and describe the question in detail with complexity. Limit the question length between 15 and 40 words.
3. The question should have practical value in real life, such as guiding people's production or daily activities.
4. The question must reflect the distinctive characteristics of the target object type, and should not be easily confused with other objects in the image.
5. Generate a reasonable answer to the question, and the answer must explicitly include the object category name I provided.
6. Output in strict JSON format, and no line breaks or other characters are allowed inside the curly braces:  
{ "description": your question, "answer": your answer }.
7. The generated questions and answers must not include phrases such as 'outlined in red'.
8. Note: If the image contains annotations for multiple red-outlined areas, the plural form of the category name should be used in the answer.
9. For specific types of aircraft or vehicles, their locations can be roughly indicated, such as in the lower right part of the image.

Here are several examples:

1. {"description": "In this industrial area near the river, exhaust gases or smoke generated during industrial processes are discharged into the upper atmosphere to dilute and disperse pollutants, thereby reducing their impact on the ground-level environment and human health.", "answer": "The chimney near the river can serve this purpose."}
2. {"description": "In this ocean area, if I want to find a small watercraft powered by jet propulsion that can glide rapidly on the water surface for recreational purposes, where should I look?", "answer": "The motorboat in the lower left part of the image meets your requirements."}
3. {"description": "In this busy residential area, where roads crisscross, which locations are prone to traffic accidents and therefore suitable for installing traffic lights and pedestrian crossings?", "answer": "The intersection in the image is a high-risk area for traffic accidents."}
4. {"description": "In this airport, which aircraft in the lower-left of image is the smaller-sized one equipped with the Pratt & Whitney PW1500G geared turbofan engine?", "answer": "The a220 aircraft is a smaller-sized plane that is equipped with the Pratt & Whitney PW1500G geared turbofan engine."}
5. {"description": "Which area in this image is suitable for 5-on-5 team sports that emphasize teamwork and coordination, where players need to perform skilled passing, screening, and movement?", "answer": "The basketball court in the lower right part of the image is suitable for 5-on-5 team sports."}

The image with red contours is provided below. The category name of target region is **category\_name**. Please analyze the image and generate a question-answer pair based on the above requirements.

Figure 6. An example of single-target QA generation prompt

## Prompt:

Assume you are an expert in remote sensing interpretation. I will provide you with a remote sensing image annotated with multiple colored outline boxes, where each color highlights a region containing a specific land cover or object type. I will also provide you with the object type represented within each color outline. Your task is to generate a pair of implicit reasoning-based question and answer according to the following rules:

1. The question must be *\*implicit\**, meaning it should not directly mention any of the provided category names. Instead, the question should require reasoning to infer the object types present in the different outlined regions.
2. You may reasonably assume or imagine a scene to construct an integrated question, or construct individual sub-questions based on each color's outline and connect them using 'and'.
3. The question must reflect *\*distinct characteristics\** of the object types in each colored region.
4. You must generate a *\*plausible answer\** to the question. The answer must include *\*all\** of the given category names.
5. Format the output as a strict JSON string with no extra characters or line breaks inside the brackets:  
{"description": your question, "answer": your answer}
6. Do *\*not\** use phrases like "outlined in red" or "outlined in blue" in the answer.
7. If a certain category appears in *\*multiple instances\** in the image, use the *\*plural\** form of that category name in the answer.
8. You may refer to spatial positions such as "in the center of the image" or "in the lower-right corner" in the question to help structure the reasoning.
9. Leverage your *\*common sense knowledge and creativity\** to generate the implicit reasoning question. The final question must implicitly involve all the categories I provide.

Below are several examples for your reference:

1. Given categories: small car, dump truck, storage tank

Output: {"description": "Which vehicles in the image are used to transport a small number of people or for self-driving tours, which ones are primarily used to carry soil or rocks, and which large structure might be used to store water or industrial materials?", "answer": "The small cars scattered across various corners of the image are suitable for personal travel or self-driving tours, the dump truck in the bottom right is used for transporting soil and rocks, and the large storage tank in the center is a facility for storing industrial materials."}

2. Given categories: basketball court, tennis court, baseball field

Output: {"description": "In this sports complex, three types of sports competitions are taking place: a game where the ball is thrown into a hoop, a rally sport involving hitting a ball over a net, and a sport where the ball is struck within a fan-shaped area. Please identify the areas where each of these sports is being played.", "answer": "The basketball court is the area for shooting the ball, the tennis court is the area for hitting the ball over the net, and the baseball field is the fan-shaped area."}

3. Given categories: a220, a330, boeing737

Output: {"description": "In this airport area, which two types of aircraft are manufactured by the European company Airbus—one being a single-aisle small passenger jet and the other a twin-aisle medium-sized aircraft—and which popular aircraft is produced by the American company Boeing?", "answer": "The a220s are small aircraft produced by Airbus, the a330s are medium-sized aircraft from Airbus, and the boeing737s is a popular passenger jet manufactured in the United States."}

The red outlined areas in the image represent *{category\_name\_1}*, the blue outlined areas represent *{category\_name\_2}*, the orange-yellow outlined areas represent *{category\_name\_3}*. Please follow the above rules to generate the question-answer pair.

Figure 7. An example of multi-target QA generation prompt

## **Categories list:**

[ "parking lot", "tree", "canal", "river", "farmland", "cooling tower shell", "cooling tower top opening", "industrial pipeline", "B1-B boomer", "airplane", "building", "terminal", "jet bridge", "sports field", "basketball court", "tennis court", "unimproved road", "center service line", "service box", "path", "baseball field", "center circle", "three-point line", "airplane engine", "hangar", "lake", "upstream", "paved square", "overpass", "sea", "storage tank", "bleachers", "ship", "harbor", "shipping container", "helipad", "airport runway", "white smoke", "dam", "driveway", "football field", "bushes", "riverbank", "road", "vehicle", "railway", "airport", "cargo hold", "volleyball court", "roundabout", "airport runway", "swimming pool", "solar panel", "dockside warehouse", "wake", "golf field", "beach", "substation", "bow of ship", "stern of ship", "zebra crossing", "no man's land of tennis court", "intersection"]

## **Prompt:**

Assuming you are an expert in remote sensing image interpretation, I will provide a remote sensing image that contains multiple closed regions enclosed by red outlines. Additionally, I will provide a list of region categories. The categories list is *{categories\_list}*. you should select a category from the list that corresponds to a red-outlined region according to the following requirements:

1. The final output must be only the object's category name. Do not include any other redundant output, such as 'the red-outlined region is...'
2. The output category name must be selected from the categories list.
3. Pay attention to the differences between similar categories, such as cooling tower shell and cooling tower top opening, path, road and road bridge, tree and bushes.
4. Before submitting your final result, please carefully verify that your category selection accurately reflects the red-outlined region and avoids any ambiguity.

## Examples:

1. If the image shows a single airplane on an airport taxiway, outlined in red. -> Output: airplane
2. If the image shows a residential area with one red contour drawn around three separate houses. -> Output: house
3. If the image shows a seaside port, and the red contour contains a warehouse-like building next to it. -> Output: dockside warehouse

Figure 8. Category generation prompt



Figure 9. More examples of LaSeRS.



Figure 10. More examples of LaSeRS.

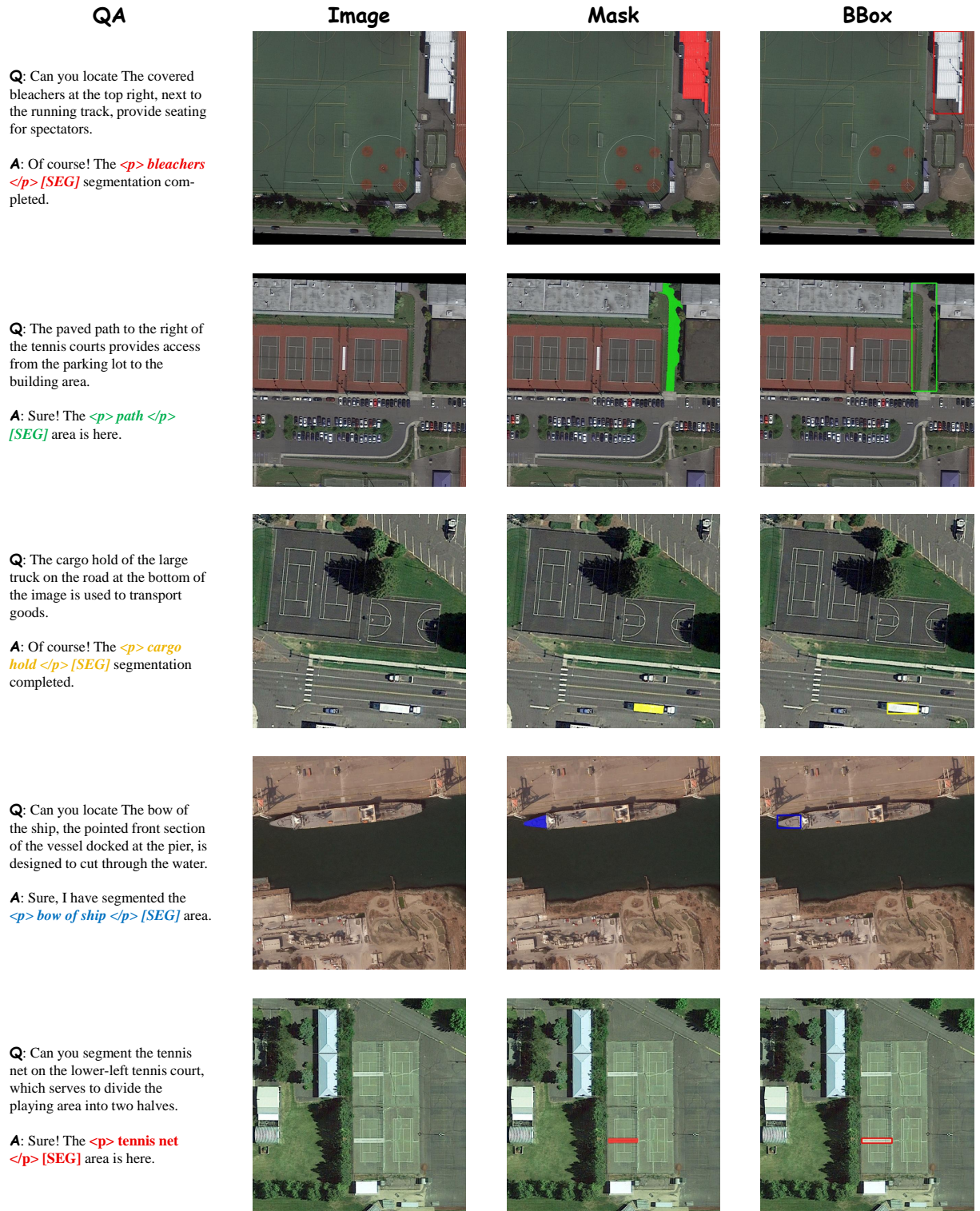


Figure 11. More examples of LaSeRS.

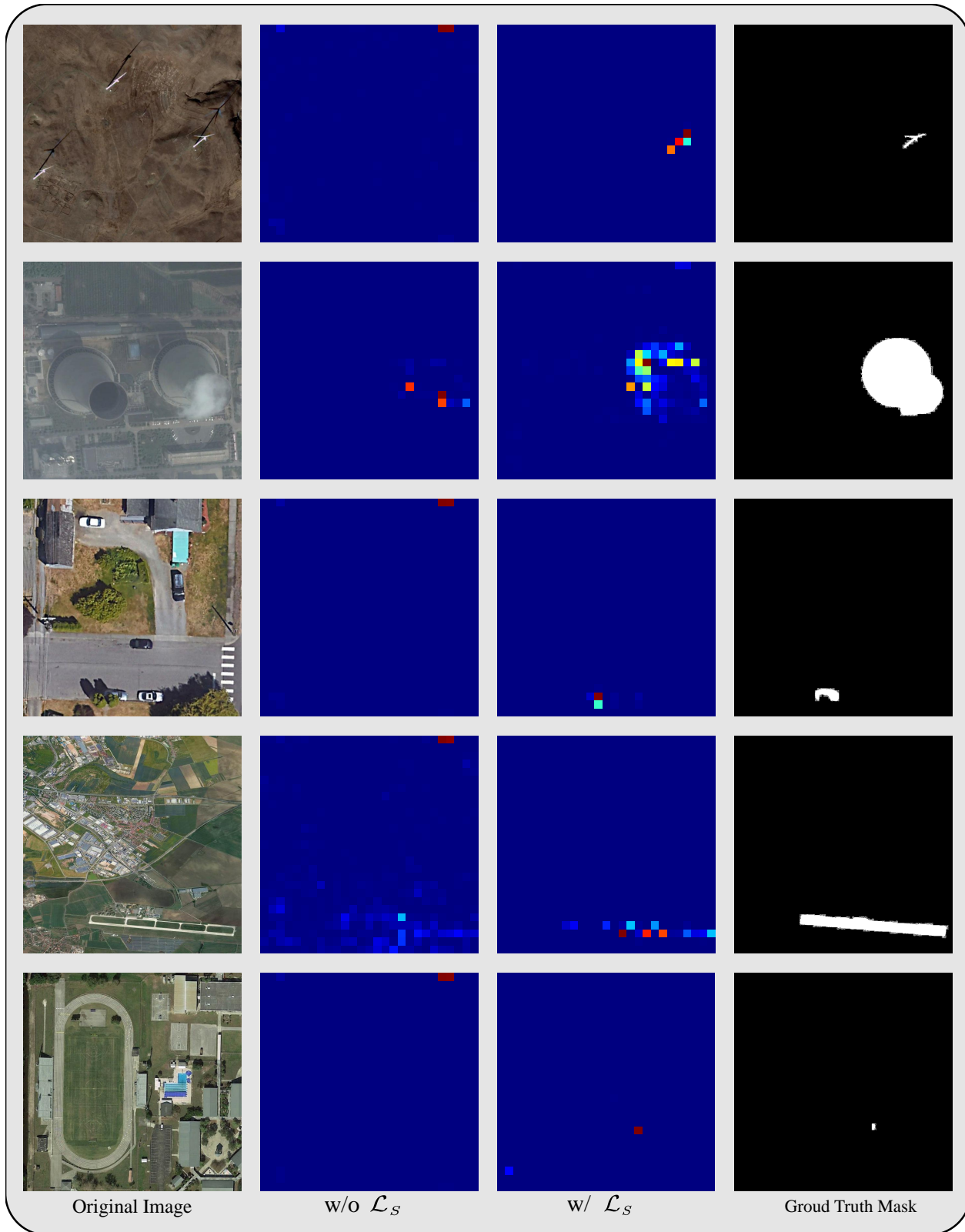


Figure 12. Additional examples of spatial attention visualizations.

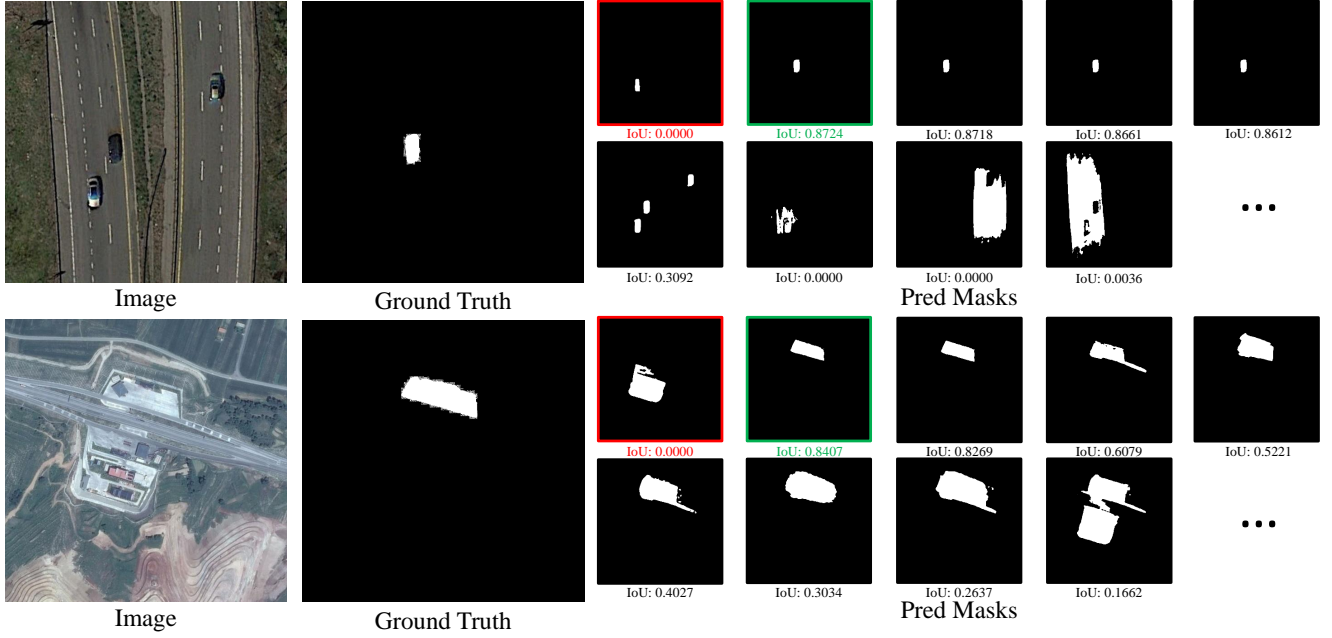


Figure 13. Visualization analysis of segmentation query number. The red box indicates the mask selected by the matching algorithm, while the green shows the mask that best matches the ground truth. It can be observed that the matching algorithm always selects a non-optimal mask, leading to a decrease in both efficiency and performance.

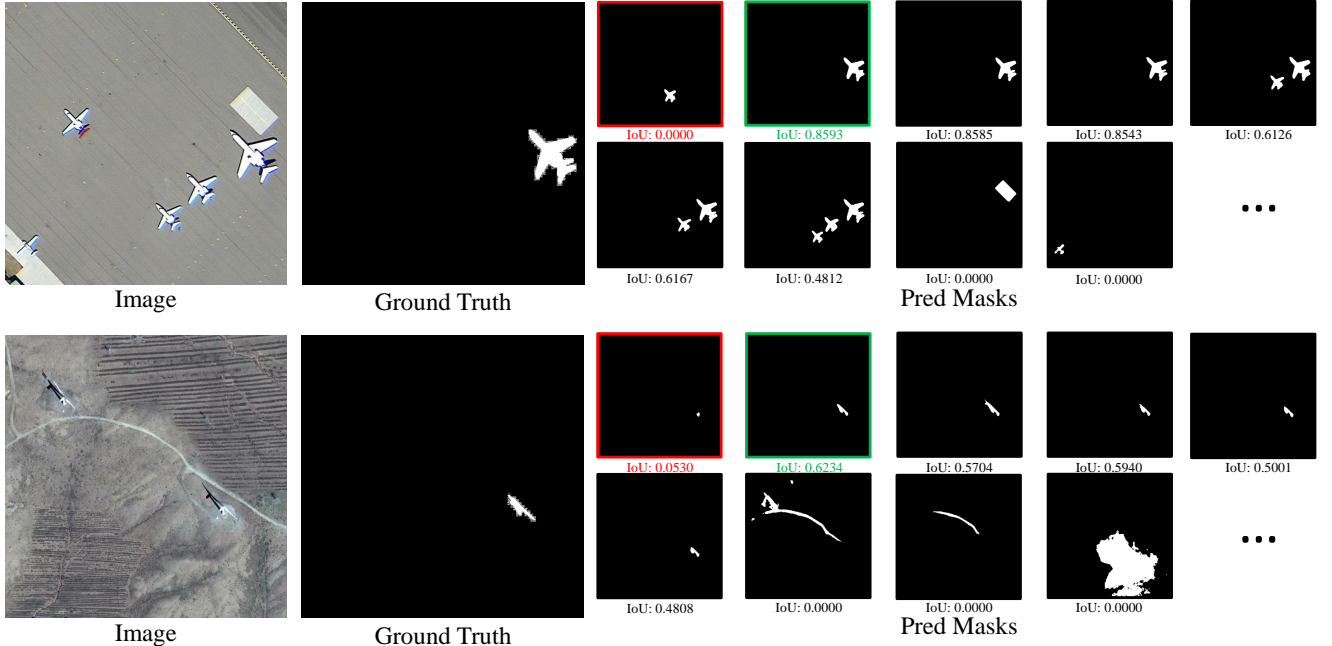


Figure 14. Visualization analysis of segmentation query number. The red box indicates the mask selected by the matching algorithm, while the green shows the mask that best matches the ground truth. It can be observed that the matching algorithm always selects a non-optimal mask, leading to a decrease in both efficiency and performance.

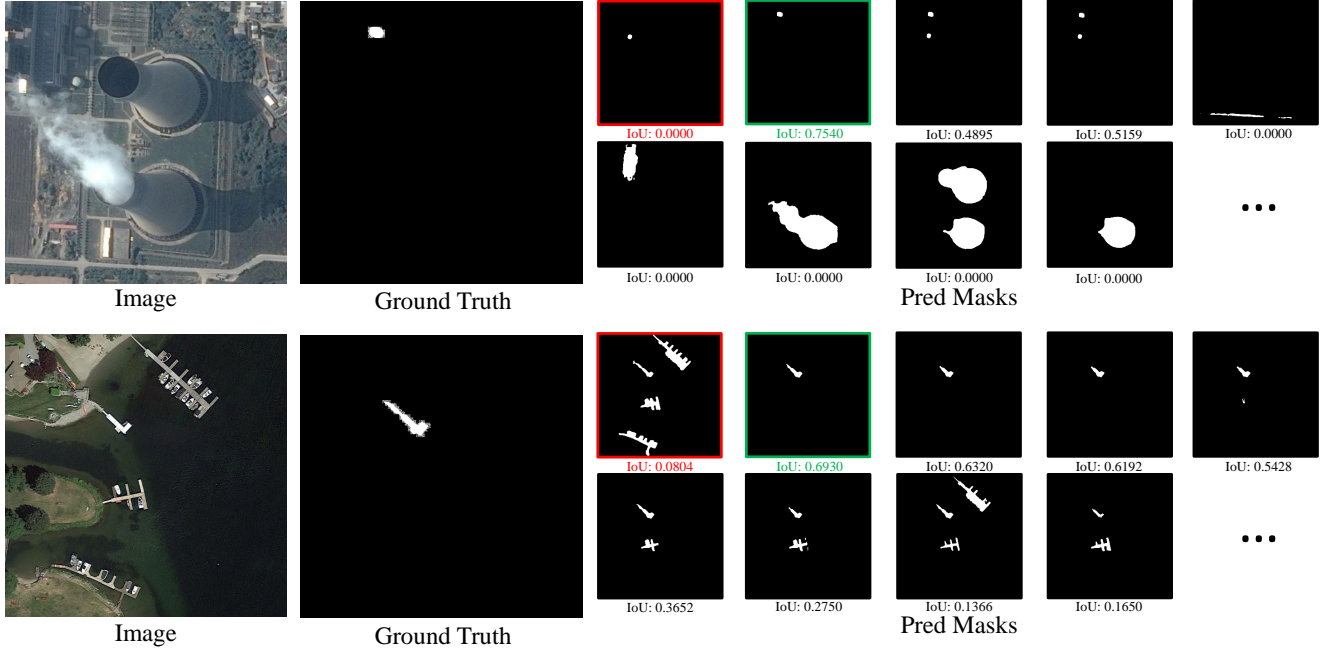


Figure 15. Visualization analysis of segmentation query number. The red box indicates the mask selected by the matching algorithm, while the green shows the mask that best matches the ground truth. It can be observed that the matching algorithm always selects a non-optimal mask, leading to a decrease in both efficiency and performance.

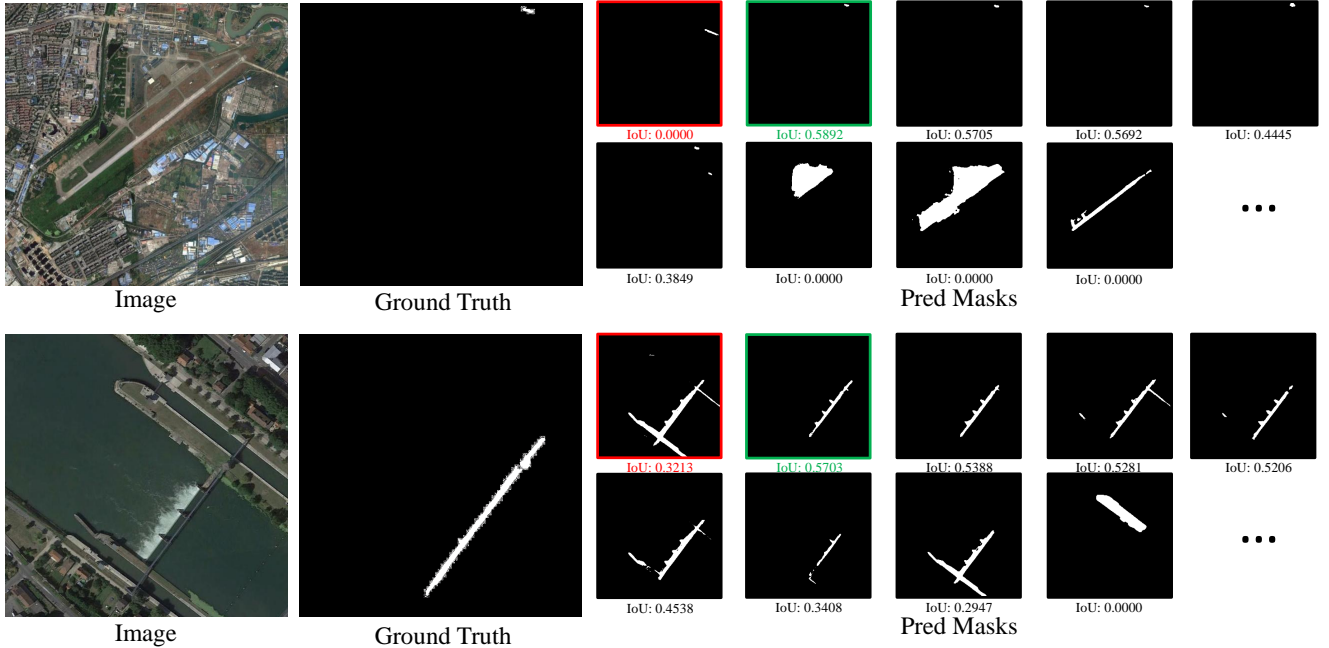


Figure 16. Visualization analysis of segmentation query number. The red box indicates the mask selected by the matching algorithm, while the green shows the mask that best matches the ground truth. It can be observed that the matching algorithm always selects a non-optimal mask, leading to a decrease in both efficiency and performance.



For a community sports day, which area is set up for a classic American team game played on a diamond-shaped infield, and which adjacent rectangular courts are prepared for racket sport matches between individuals or pairs?



The structures designed for the large-scale containment of fluids are the **storage tanks** [SEG], and the **bridge** [SEG] provides essential connectivity by spanning the waterway.



The area for the classic American team game is the **baseball field** [SEG], and the adjacent rectangular courts are the **tennis courts** [SEG].



In this port, what types of vehicles and equipment work together to handle the allocation and transportation of various resources?



For a risk assessment of this waterside industrial complex, which structures are designed for the large-scale containment of fluids, and what single structure provides essential connectivity for transport or utilities by spanning the waterway?



In this port, the large **ship** [SEG] docked at the shore handle the transport of bulk cargo, while the three **small vehicles** [SEG] on the dockside are used for moving light equipment and personnel.



To ensure the security of the global energy supply chain, we need to monitor key infrastructure. In this coastal industrial zone, what are the large cylindrical structures on the left used for stockpiling petroleum or chemical products, what is the man-made structure extending into the sea that allows for the loading and unloading of these products, and what type of large marine vessel is used to transport them internationally?



The large **storage tanks** [SEG] on the left are used for stockpiling petroleum or chemical products. The **harbor** [SEG] is the structure that extends into the sea for loading and unloading. The **ship** [SEG] is the marine vessel used for international transport.

Figure 17. Visualization results of SegEarth-R2 on the LaSeRS dataset.

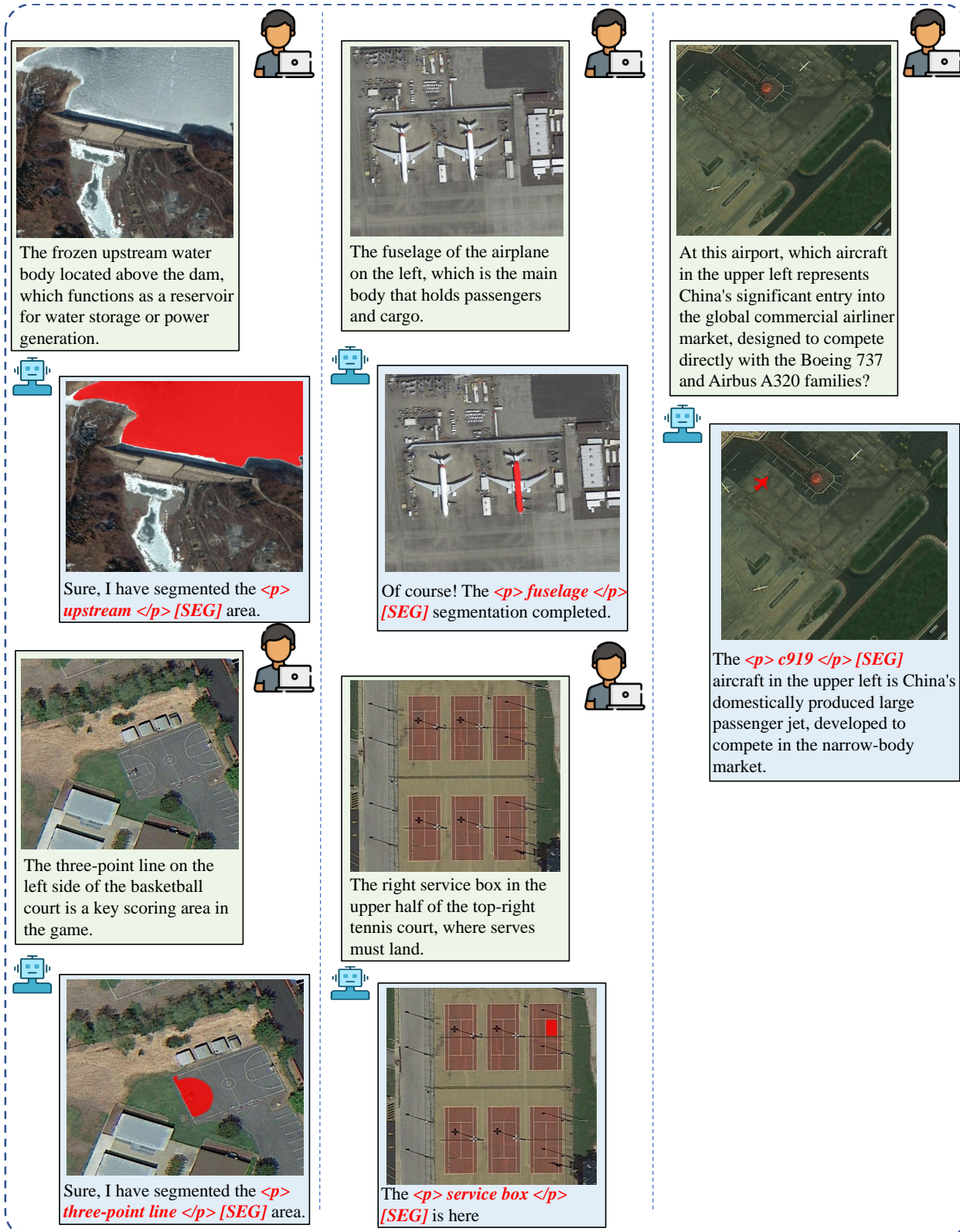


Figure 18. Visualization results of SegEarth-R2 on the LaSeRS dataset.



Figure 19. Visualization results of SegEarth-R2 on the RefSegRS test set.



Figure 20. Visualization results of SegEarth-R2 on the RRSIS-D test set.

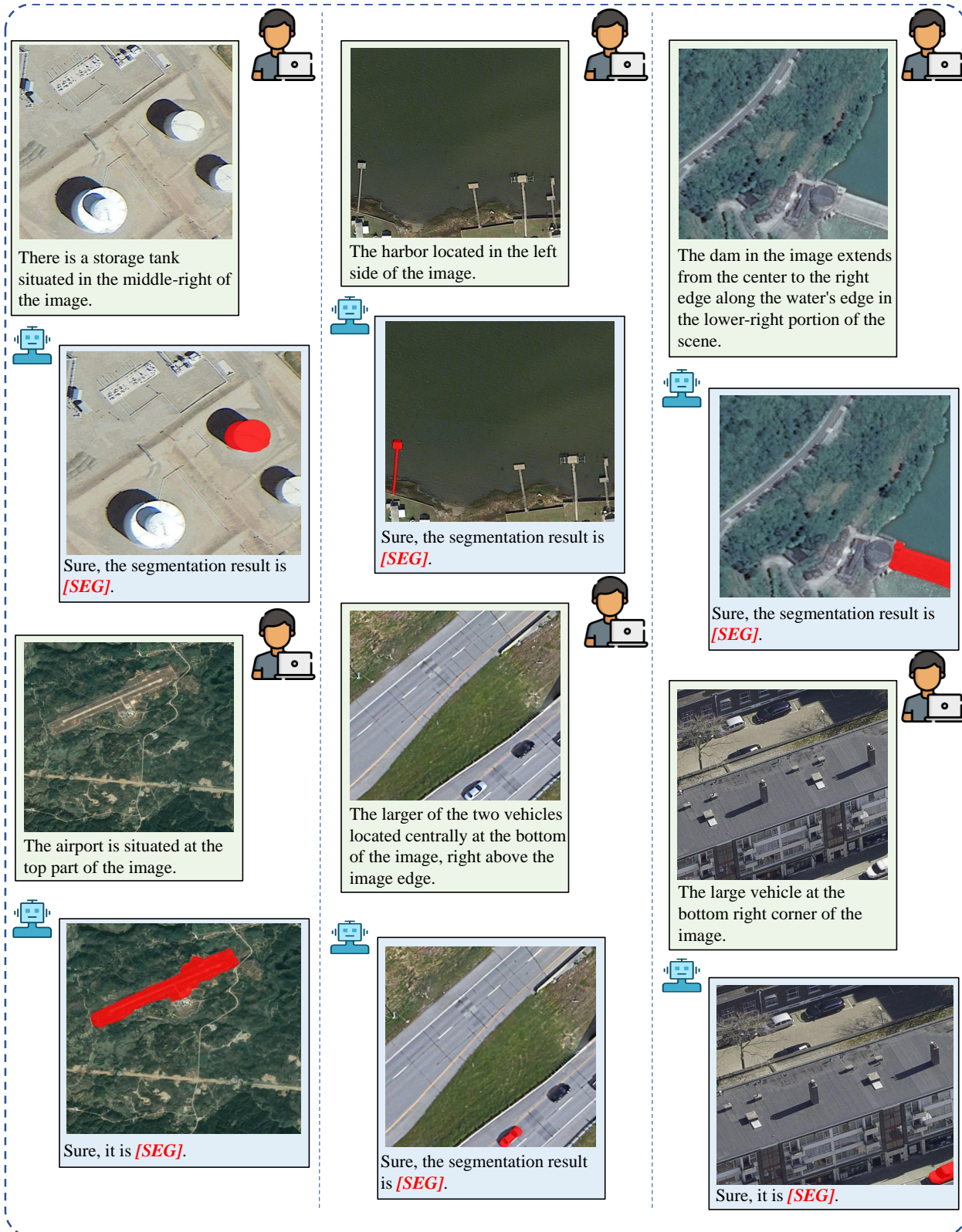


Figure 21. Visualization results of SegEarth-R2 on the RISBench test set.



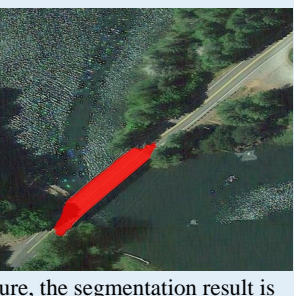
In the event that an emergency medical evacuation is necessary in a secluded wooded region, which location would be best for helicopter landing?



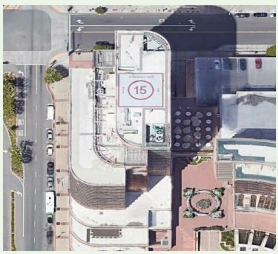
Sure, the segmentation result is **[SEG]**. The helipad, positioned atop the building, offers a direct landing zone for helicopters, ensuring swift entry during urgent situations.



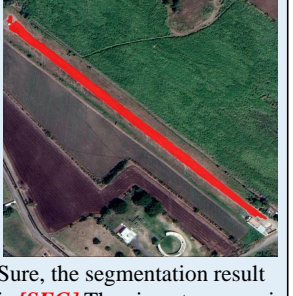
What kind of construction enables individuals to traverse a body of water, linking two distinct regions for transportation and commerce?



Sure, the segmentation result is **[SEG]**. The bridge, with its graceful structure, plays a crucial role in uniting two separate locations, ensuring that crossing the water is both simple and effective.



In the event that an emergency medical team must urgently access the building's rooftop, which spot will they utilize?



Sure, the segmentation result is **[SEG]**. The airport runway is meticulously engineered and cared for to facilitate the safe takeoff and landing of aircraft, promoting both security and operational effectiveness.

Figure 22. Visualization results of SegEarth-R2 on the EarthReason test set.